DESIGN AND MANUFACTURING OF NOVEL HYBRID METAL-POLYMER HEAT EXCHANGERS

BY

GOWTHAM KUNTUMALLA

THESIS

Submitted in partial fulfillment of the requirements
for the degree of Master of Science in Mechanical Engineering
in the Graduate College of the
University of Illinois at Urbana-Champaign, 2020

Urbana, Illinois

Adviser:

Associate Professor Sanjiv Sinha

ABSTRACT

In the United States, over 50% of the unrecovered energy from industrial processes is in the form of low-grade heat ($200°C$). Materials and maintenance costs of common heat exchangers are typically too high to justify their usage. Polymers, though more affordable, are usually unsuitable for heat exchanger applications due to their low thermal conductivity ($\sim 0.2\ W/mK$). Here, we show that metal-polymer hybrids may be attractive from both performance and cost perspectives. The use of polymers further increases the resistance to corrosion by sulfuric and carbonic acids often present in flue gases. This work explores manufacturing different configurations of layered polyimide-copper macroscale hybrids for heat exchanger applications using a modified roll to roll process. We created a manufacturing pathway for producing such layered hybrid tubes that involves directly rolling and bonding tapes made of polymer and copper foil into tubes. A critical problem in the fabrication process is the bonding of metal and polymers. We explore approaches involving adhesives (epoxy, acrylic , and silicone) for metal/polymer interfaces and direct welding (ultrasonic) for metal/metal interfaces that can be integrated into the manufacturing process. We report characterisations of the thermomechanical properties of these joining processes. This work paves way for realizing cost effective manufacturing of heat exchangers for low-grade waste heat recovery.

To my Parents and Sister, for all their love and support

ACKNOWLEDGMENTS

TABLE OF CONTENTS

NOMENCLATURE

Adh	Adhesive
APW	Acousto-plastic welding
CF	Cold fluid
Cu	Copper material/foil
U_{eff}	Overall heat transfer coefficient
HX	Heat Exchanger
M/M	Metal/Metal joint
M/P	Metal/Polymer joint
Poly	Polymer
l_{Cu}	Length of copper layer
l_o	Length of overlap
l_{poly}	Length of polymer layer
t_{Cu}	Thickness of copper layer
t_{poly}	Thickness of polymer layer
t_{wall}	Thickness of wall
R2R	Roll to Roll process
RSW	Resistance seam welding
USW	Ultrasonic welding

CHAPTER 1

INTRODUCTION

1.1 Motivation

Low-grade heat ($<200°C$) comprises between 50 to 60% of the unrecovered energy from industrial processes [1]. Traditional all-metal heat exchangers (HX) are typically too expensive for such applications where the payback period is less than 3 years [2]. Further, corrosion due to condensed sulfuric and carbonic acids at temperatures $<150°C$ creates additional problems for metallic HX [3]. The use of polymers in low temperature HX can reduce costs and provide better resistance to corrosion. However, polymers remain unsuitable due to their low thermal conductivity ($\sim 0.2\ W/mK$). The low conductivity leads to a high wall thermal resistance that limits the overall heat transfer coefficient.

1.2 Prior Work

Recent work has explored several approaches [4–9] for enhancing the thermal conductivity of polymers. Wang et al.[8] used high modulus, thin polymer fibers and measured thermal conductivity along the fibers. This approach is not beneficial in the case of heat exchangers due to the requirement of heat conduction in the transverse direction. Choy et al. [9] have proposed ultra-drawn polyethylene. Though the axial tensile modulus and axial thermal

conductivity increase in this approach, properties along the transverse directions suffer. Roy et al.[7] demonstrated improved thermal conductivity of thin film polymer brushes in the cross-plane direction but the extremely low thickness ($40nm$) of the material limits its use in practical applications. The more common approach of [5, 10] dispersing metal particles during polymerization of thick polymers ($>1mm$) yields high thermal conductivity ($\sim 10 - 12\ W/mK$). These metal-polymer micro-mixtures show as high as 60% reduction in tensile strengths due to air inclusions. Further, the order of magnitude difference in the thermal expansion coefficient of the metal particles versus the typical polymer matrix leads to thermomechanical hysteresis [6].

1.3 Metal-Polymer Hybrid HX

To overcome the above issues, we describe a different approach here: a macroscale metal-polymer hybrid that separates the heat conduction pathway between metal and polymer such that heat essentially flows in parallel circuits across the two materials. This specifically reduces the impact of the large thermal interfacial resistance between metal and polymer. In a tube formed from the material, heat conduction is short-circuited from the hot to the cold side across the HX walls through the metal while the polymer provides the mechanical scaffold for the HX tube. Figure 1.1 illustrates the basic idea behind the approach. The polymer strips act as a scaffold for an extended copper surface that is also formed from a thin foil. When the combination is subject to convection on the two sides, the heat flow lines indicate that the heat is shunted through the copper. This two-dimensional structure can be thought of as the surface of a three-dimensional hollow tube, which can be fabricated
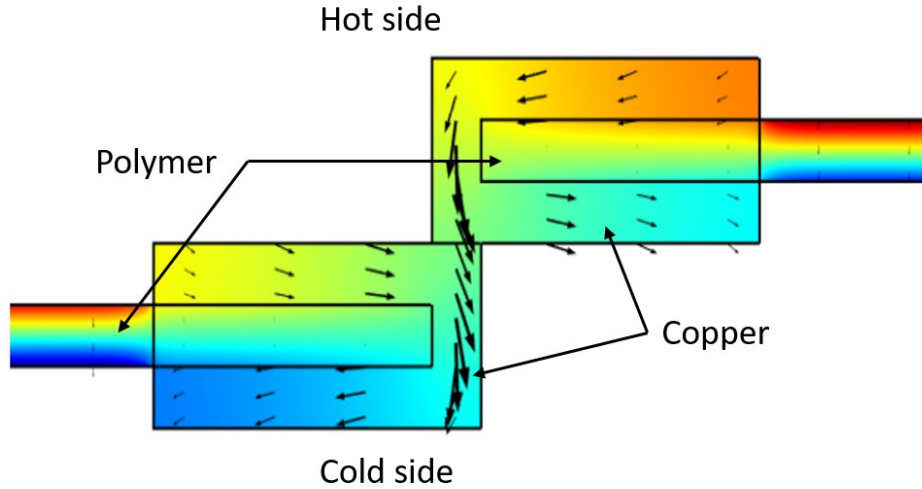
Figure 1.1: Basic idea behind macroscale HX. Arrows indicate direction of heat transfer.

by wrapping polymer and copper strips together. For example, a helical wrapping of metal and polymer strips can be done in a roll to roll (R2R) process. More such configurations are discussed in detail in the following sections. The strategic placement of copper and polymer strips ensures that the overall heat transfer coefficient is not limited by the wall thermal resistance.

Two key challenges in this approach are

1. Retaining the heat transfer pathways i.e. reasonable effective thermal conductivity.

2. Maintaining thermomechanical strengths for safe operation.

In a separate paper, [11] we discuss the first challenge in detail. In that work, through numerical simulations, we obtain copper-polymer geometries that achieve a viable wall thermal conductivity $\sim 1\ W/mK$ at $\sim 23\%$ volume fraction of copper. The enhancement in thermal conductivity is also around $\sim 23\%$ compared to all polymer heat exchangers. Computer simulations show that under the normal operating conditions of the heat exchanger, these

3

hybrid pipes can withstand >200 *psi* internal pressures. In the current work, we explore solutions to overcome the second challenge: the critical problems of bonding the metal to polymer and metal to metal. Some part of this thesis has also been published in ASME 2019 conference proceedings [12]. Prior work has extensively investigated different methods of joining metals to polymers [13–18]. The high fluidity of adhesives and their ability to form strong bonds between specific metals and polymers under sufficient applied pressures is particularly useful in this work. Such bonding is also suited to the curved interfaces that are encountered in this work. Finally, the speed at which the bonding can be performed is an added advantage. Hence, we consider joining metal to polymer using adhesives (epoxy, acrylic , and silicone). We further explore ultrasonic welding for joining metal to metal as a first step. Other choices such as laser and resistive welding are possible avenues for future work.

1.4 Structure of the Thesis

This thesis is organized as follows. Chapter 1 gives an overall description of the problem statement. Chapter 2 describes the various configurations and joining techniques for metal polymer hybrid heat exchangers, that we came up with. Chapter 3 discusses the results obtained from the thermomechanical experiments conducted on samples made using these materials and methods. Chapter 4 consists of details about Roll to Roll (R2R) manufacturing setup built in-house at UIUC. Chapter 5 shows the results of the performance of HX in a wind tunnel apparatus. Chapter 6 summarises the findings of this project and give broad directions for the future scope of work. Overall, we conclude that the innovative joining

techniques for metals polymer hybrids, presented here, are promising. This work paves way for realizing cost-effective manufacturing of heat exchangers for low grade waste heat recovery.

CHAPTER 2

DESIGN OF HYBRID TUBES

2.1   Idea of Macroscopic Joining

In the current study, materials under consideration are (1) Copper as the metal and (2) DuPont ^{TM} Kapton$^®$ HN film (a polyimide) as the polymer. Thickness of the polymer is 2 mils ($\sim 50~\mu m$). Copper 1181 conductive tapes with a thickness of 1-10 mils ($\sim 25 - 250~\mu m$) are used for adhesive joint tests and 110 Copper foil with a thickness of 1-10 mils ($\sim 25 - 250~\mu m$) are used for Ultrasonic weld joint tests. These materials meet ASTM B152 standards. Joints are described in subsection 2.2. In further sections, the words metal and copper are used interchangeably. Copper is chosen for its high thermal conductivity ($400~W/mK$) and polyimide for its high temperature stability ($200~°C$). Further, the linear thermal expansion coefficients of the materials are comparable ($17~ppm/°C$ for copper and $20~ppm/°C$ for polyimide).

2.2   Various Configurations

Figure 2.1 illustrates various tape geometries that can yield an HX tube upon proper procedural bonding. The red arrows in the figure indicate the places where joining is required. As discussed earlier, possible joining techniques include adhesive bonding and seam welding.
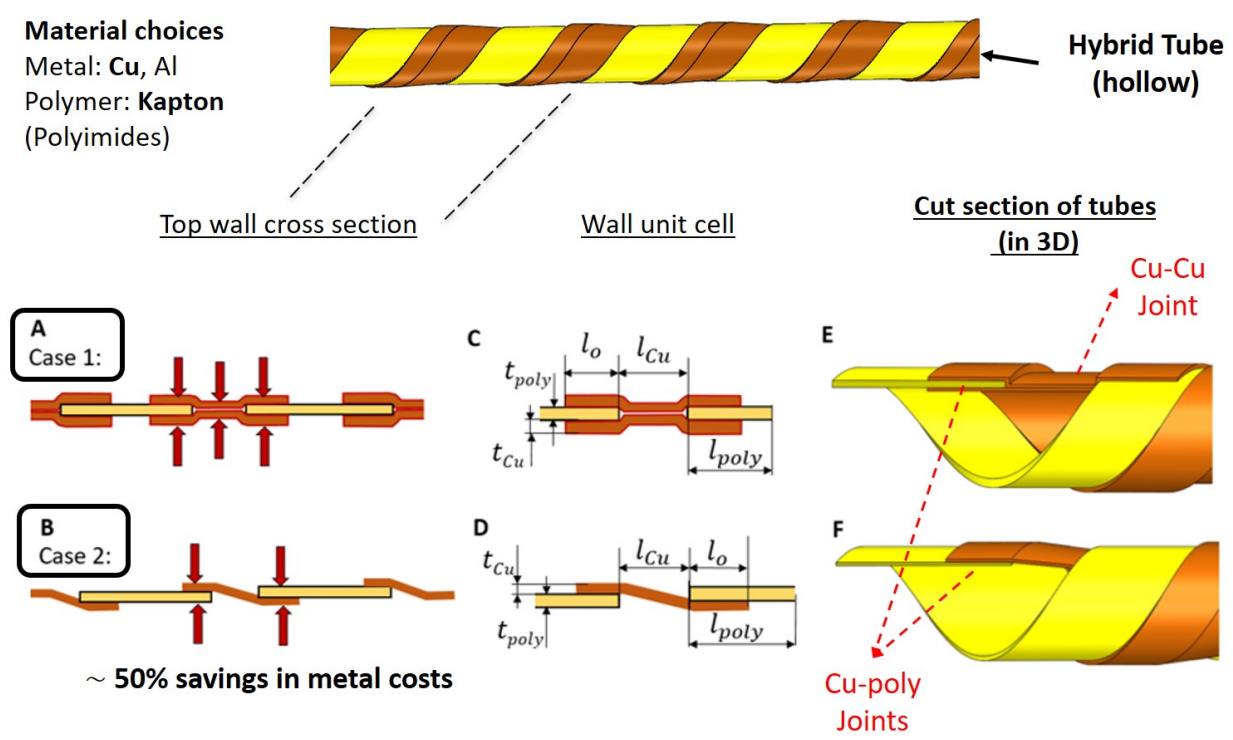
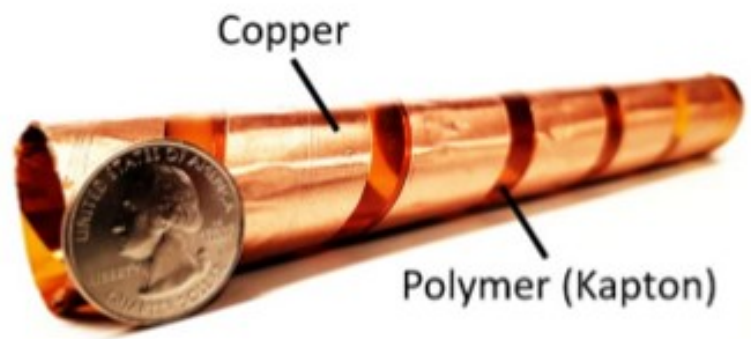Figure 2.1: Various Configurations of Hybrid Heat Exchanger tubes

Figure 2.2: Actual hybrid tube made at UIUC

Figure 2.3: HX example using staggered configuration stack of hybrid tubes

The important geometric dimensions are the lengths $(l_{Cu},\ l_{poly})$ and thicknesses $(t_{Cu},\ t_{poly})$ of copper and polymer layers. The length of overlap (l_o) determines the relative positions of these layers. Figure 2.2 shows a real tube, in case 1 configuration, made at UIUC using a custom apparatus. Figure 2.3 is staggered configuration stack of hybrid tubes. These tubes can be connected in parallel or series combinations.

2.3 Joining Methods

Cases 1, 2 and 3 have both copper/copper and copper/polymer joints. Case 4 is much simpler and contains only copper/polymer joints. These joints when formed should hermetically seal a cylindrical tube. To make the metal/metal joints in a continuous process, we initially considered three welding techniques namely ultrasonic, laser and resistance seam welding. Laser welding is a challenging task for joining copper to copper. This is because of the high thermal conductivity and high surface reflectivity of copper [14],[15]. Ultrasonic welding
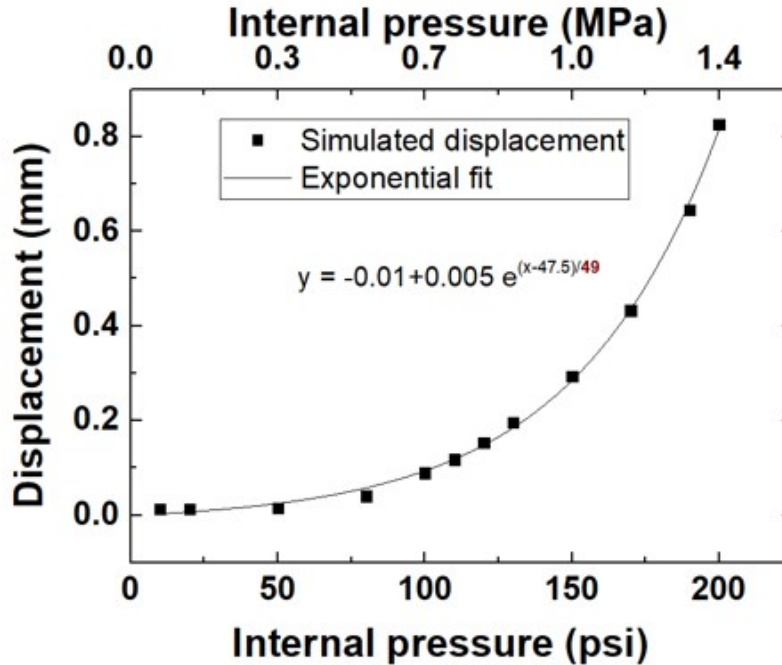
Figure 2.4: Internal strength requirements. Picture taken from [11].

(USW) is a fast and economic approach for joining copper to copper as well as copper to polymers [15]. We note that in general, USW is not associated with joining metals to polymers but can yield potential savings in operational costs. High heat generation is likely to be an issue in resistance welding of copper to copper in our designs because of the copper being adjacent to the polymer. The other joint, between the copper and the polymer, was made using adhesive bonding (acrylic, epoxy and silicone). A necessary design constraint for these joints comes from the internal strength requirements in a fluid flow situation. Figure 2.4 illustrates the displacement of dissimilar joints modelled using a Cohesive Zone Delamination (CZM) method [11]. A 0.2 mm limit on displacements yields a maximum internal pressure of about 125 psi.

CHAPTER 3

THERMOMECHANICAL CHARACTERISATION

The joining techniques described in the previous chapter can potentially be used to realize the heat exchangers shown in the Fig. 2.1. For large scale integrated production, these tubes can be made in a roll to roll process involving helical wrapping of copper and polymer strips and simultaneous application of joining methods. Metal-metal joints are easier to form and are typically stronger than joints between metals and polymers. From our earlier discussion, it is obvious that the copper/polymer joints play a limiting role in the structural integrity of the heat exchangers. Prior work [16, 17] provides an in-depth analysis of fracture mechanics in metal polymer hybrid materials. Delamination is the primary mode of failure in these hybrid materials [18].

Two common modes of failure are considered in this paper: (1) Opening or Peel or Tensile or Mode 1 and (2) Shear or Mode 2. Figure 3.1 shows the 2-dimensional block diagram of these thermomechanical tests. Peel strength is generally used to measure the bond strength of adhesive joints and is the average load per unit width of bond line required to separate bonded materials where the angle of separation is 180 degrees. It is usually denoted in N/cm or pounds/inch. In contrast, a shear load tends to produce a sliding failure on a material along a plane that is parallel to the direction of the force. It is usually denoted in MPa.
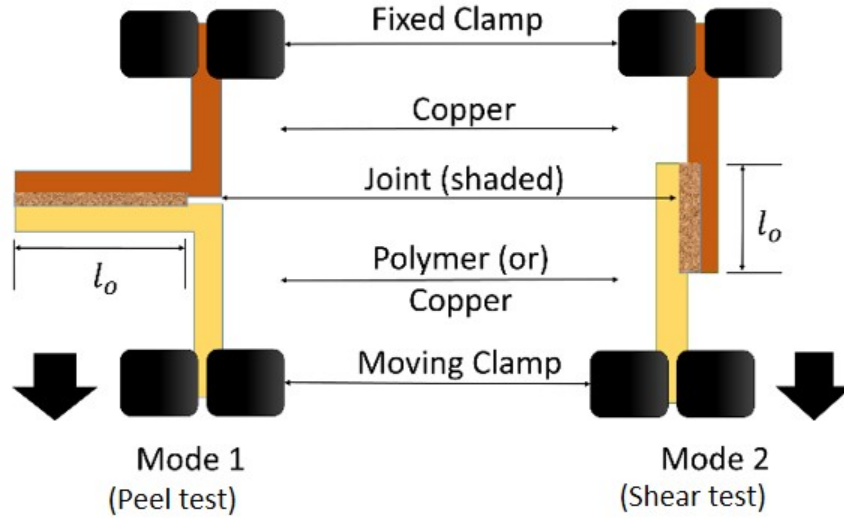
Figure 3.1: Peel test and Shear test. Black arrow indicates direction of movement of bottom clamp.

3.1 Ultrasonic Welding

A Branson Ultraweld L20 Spot Welder was used in this study to perform USW. Energy mode and welding cycles were selected to reach the specified energy. USW is used for making metal/metal interface samples. The diameter of the weld spot is 8mm across all the samples.

3.2 Adhesives

Epoxy (4540N) adhesives were obtained from Cotronics, Inc. Native adhesives present on the copper and polyimide foil tapes are acrylic and silicone respectively. These adhesives were used for making metal/polymer interface samples. The thickness of each adhesive is approximately 1.2 mils ($\sim 30 \mu m$).

3.3 Testing Method

To measure the bond strength of both M/M and M/P joints, we performed thermomechanical tests on sample specimens made using these joining methods. Peel and Shear tests were performed on a high accuracy Instron universal testing machine (model 1332) with digital data output. Figures 3.2, 3.3 show a typical test coupon fixed in the universal test machine (UTM). Since the heat exchanger is designed to perform in a hot air environment, these tests were performed at different air temperatures. A hot air blower (Tacklife, 1700 W, 50-650°C, 250-500 L/min), was used to create the necessary experimental conditions. Two thermocouples were attached to the test specimen, one facing the hot air side and one on the other side of the sample. These thermocouples provided the surface temperature of the samples. They were mainly used to check the flow conditions (by calculating the average temperature of the joint) across the different sets of experiments.

Table 3.1: Thermomechanical Tests

Test type	Amplitude of Single Ramp test (mm)	Ramp slope (mm/sec)	Sampling frequency (ms)	Repeats (n)	Material thickness (mils)	Joint dimensions
Adh-Peel	90	4.5	20	5	Cu - 1 mil, Poly - 2 mils	3 cm x 2.54 cm
Adh-Shear	5	0.2	10	5	Cu - 1 mil, Poly - 2 mils	5 cm x 2.54 cm
USW-Peel	35	1	10	4	Cu - 10 mils	8 mm dia.
USW-Shear	8	0.3	10	10	Cu - 10 mils	8 mm dia.
USW-Shear	8	0.3	10	10	Cu - 8 mils	8 mm dia.

Table 3.1 shows the experimental conditions. It is important to note that the surface conditions and curing parameters affect the strength of adhesive bonds. For the sake of consistency, all adhesive joint samples were cured at room temperature for 24 hours under a positive pressure of approximately 650 gm-force per sample. Post curing was performed at 125°C for 90 minutes. This ensures the completion of any microstructural changes which occur at dissimilar surfaces.

3.4   Results and Discussion

In this section, we present results from thermomechanical testing and discuss the implications.

3.4.1   Metal/Polymer Joints - Adhesives

Figures 3.4 and 3.5 show typical load curves for the peel and shear tests, respectively, in metal-polymer adhesive joints. The maximum values of the peel strength and shear strength are reported in Figures 3.6 and 3.7, respectively. The error bars indicate the variance in repeated experiments. Both the peel and shear strengths of the adhesive joints decrease with an increase in temperature, as expected. This can be attributed to the softening of the adhesives (essentially made of polymers) at higher temperatures. Acrylic is a thermoplastic material which melts and re-flows at high temperature. It has a superior peel strength that decreases rapidly with an increase in temperature. Further acrylic degasses and produces poisonous fumes above 150°C. Hence, it is not recommended for use in its current form. Silicone is another choice of bonding though the high variability and thus, poor reliability
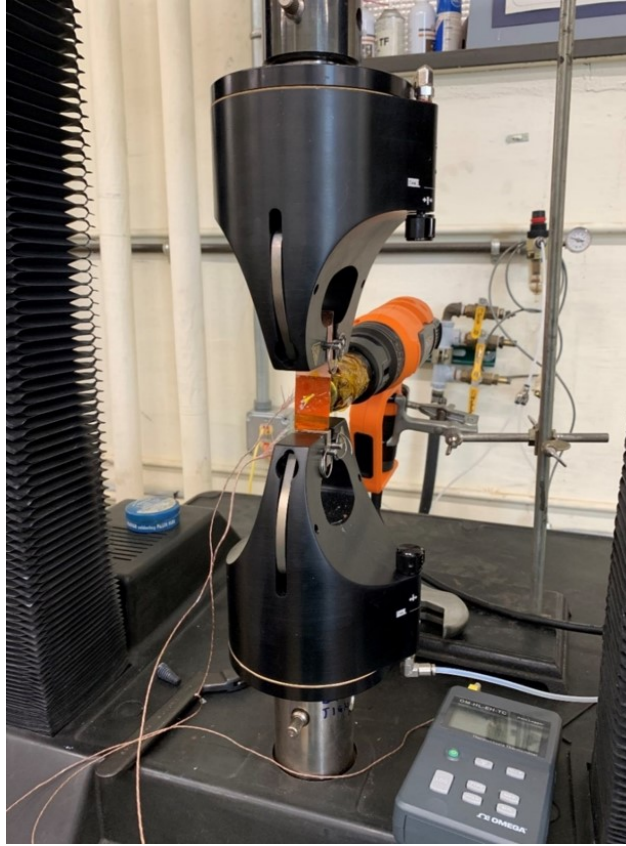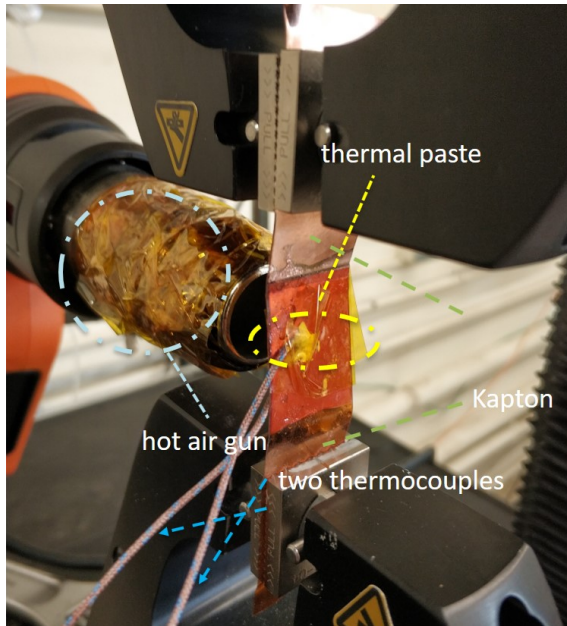
Figure 3.2: Universal Testing Machine (UTM)

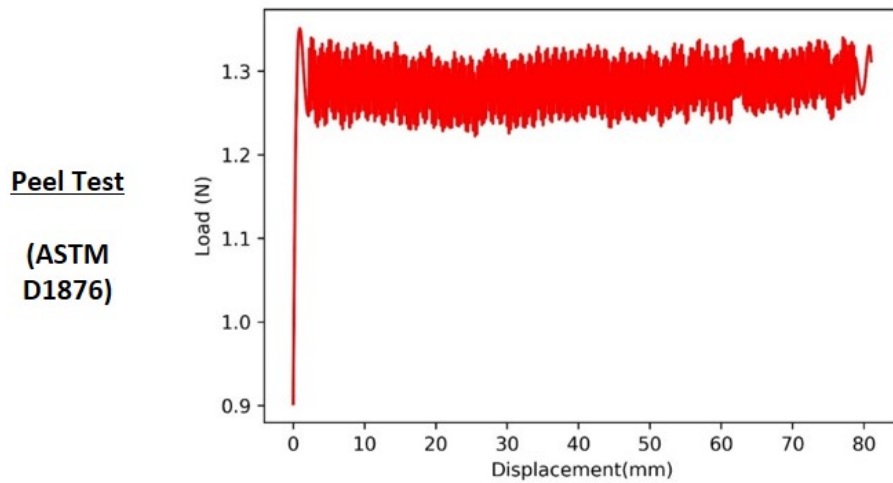Figure 3.3: Closeup of test coupon fixed in a UTM

Figure 3.4: Example load curve of a peel test of an adhesive joint

in bond strength, rendering it a poor choice. Epoxy is a thermoset polymer which forms a permanent rigid M/P bond which also provides structural strength in a cylindrical geometry. Epoxies appear to be a good choice based on these tests.

Peel tests are inconclusive due to low confidence in results. For more concrete proof, both Cu/Cu and Cu/Kp joints were further shear tested using Epoxies only. This testing using Epoxies yielded good results. Figure 3.8 summarises shear test results of epoxy bonds between Copper and Kapton. Whereas figure 3.9 shows the same between Copper strips.

3.4.2 Metal/Metal Joints - Ultrasonic Welding

Figures 3.10 and 3.11 show typical load curves for the peel and shear tests respectively in metal to metal USW joints. The diameter of the weld spot is 8mm across all the samples. The error bars indicate the variance across experiments. The nature of the peel load curve can be explained by the mesh nature of the USW. Initially, the bonds break one strand segment after another resulting in an oscillatory trend in the strength-displacement curve.
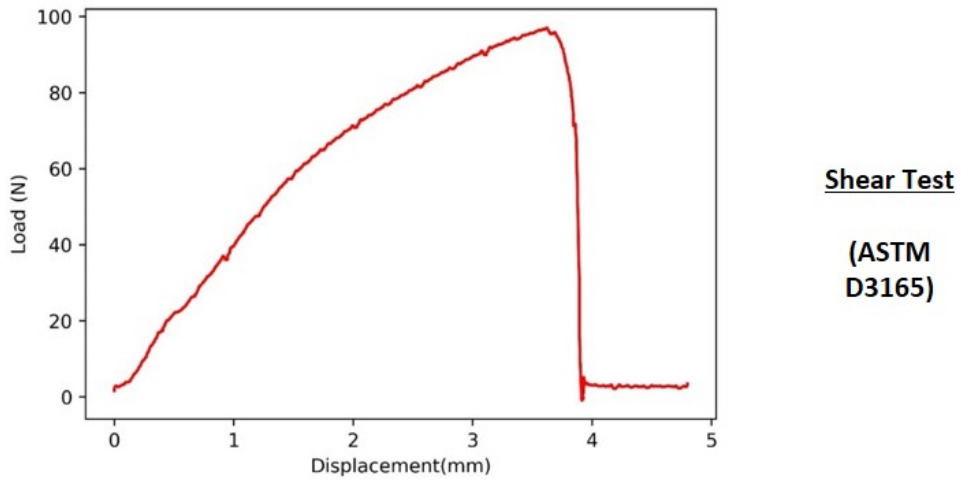
16

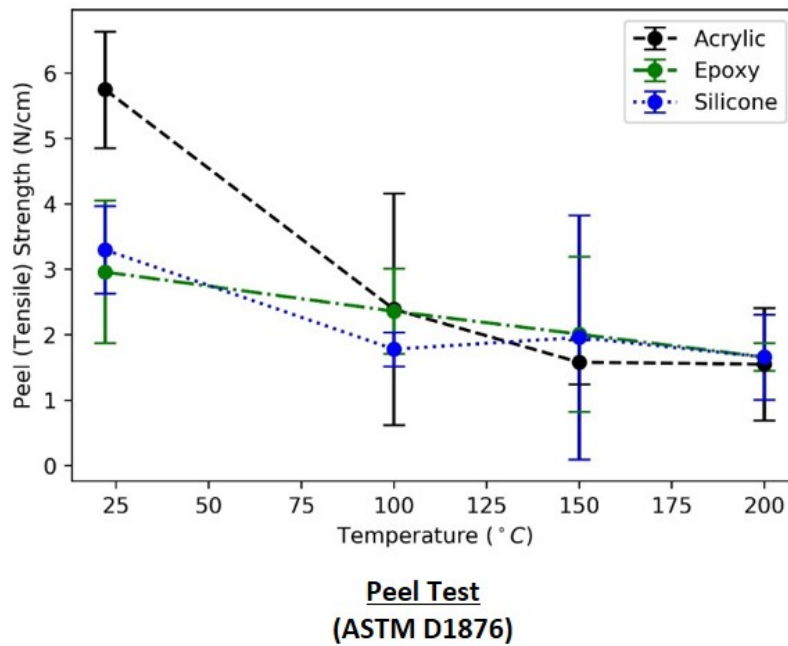Figure 3.5: Example load curve of shear test of an adhesive joint

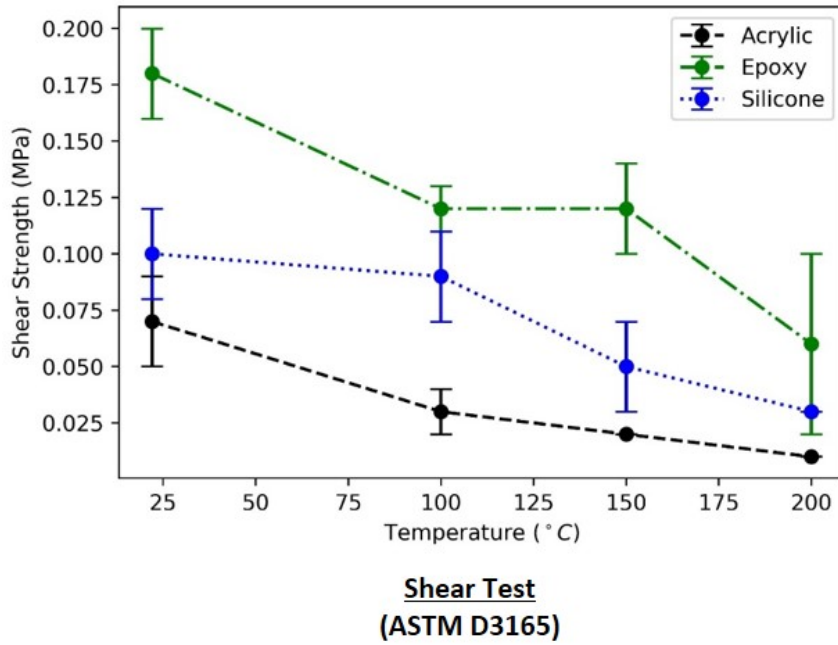
Figure 3.6: Results of peel tests of adhesive joints

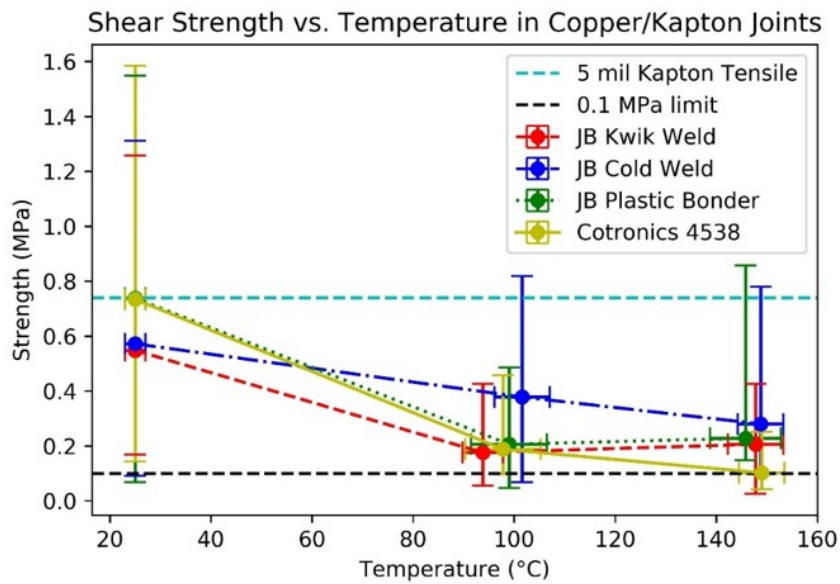Figure 3.7: Results of shear tests of adhesive joints

Figure 3.8: Results of shear tests of Epoxy joints in Copper/Kapton coupons
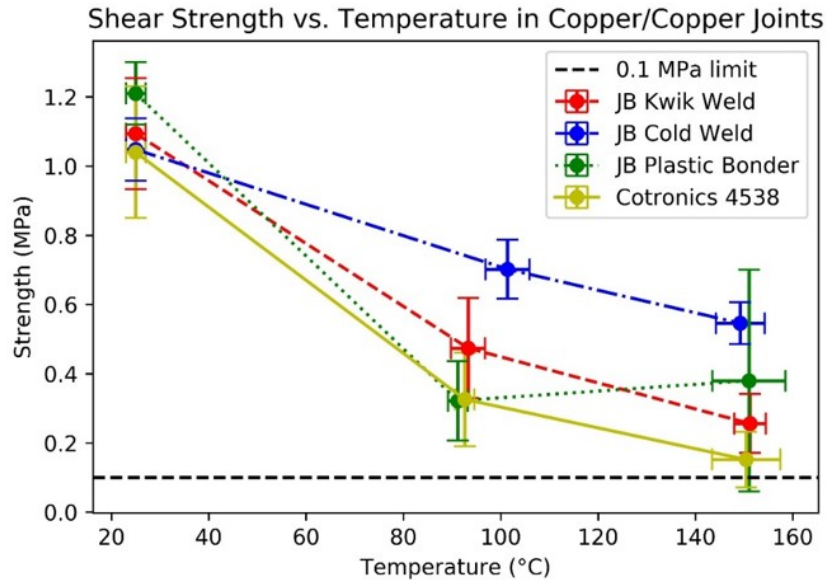
Copper/Copper Joints

Figure 3.9: Results of shear tests of Epoxy joints in Copper/Copper coupons

This trend is consistent across the samples and acceptable. We report the peel strength for spot welds in terms of peak load, consistent with the literature. Peel strength can be calculated, for comparison with adhesive, by normalizing the peak force with the weld diameter of 8mm. Reporting this value in N/cm may not be the most appropriate measure because of the failure of joint in two successive modes, namely failure in mesh region and failure in heat affected zone. But this will give a broad picture about the strengths for comparison purposes.

We performed all these tests at room temperature (25°C) only. This is mainly to measure the strengths relative to the adhesive joints. Welding was performed using a mix of weld amplitudes and weld times to further identify optimal welding conditions. Figure 3.12 shows the peel strength data. A simple calculation shows that the peel strength of M/M USW joints, on an average, is higher by two orders of magnitude, compared to the M/P adhesive
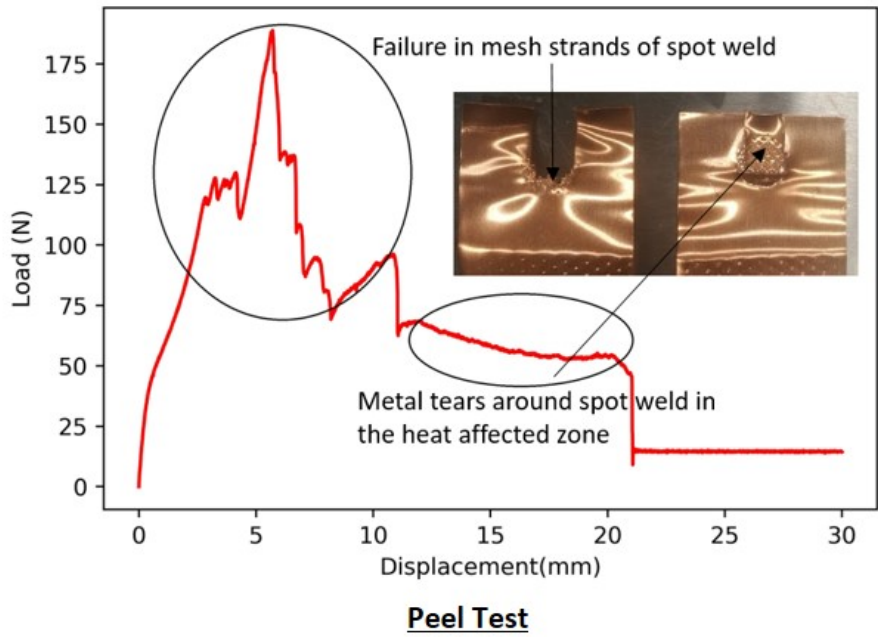
Figure 3.10: Example load curve of a peel test of a USW joint
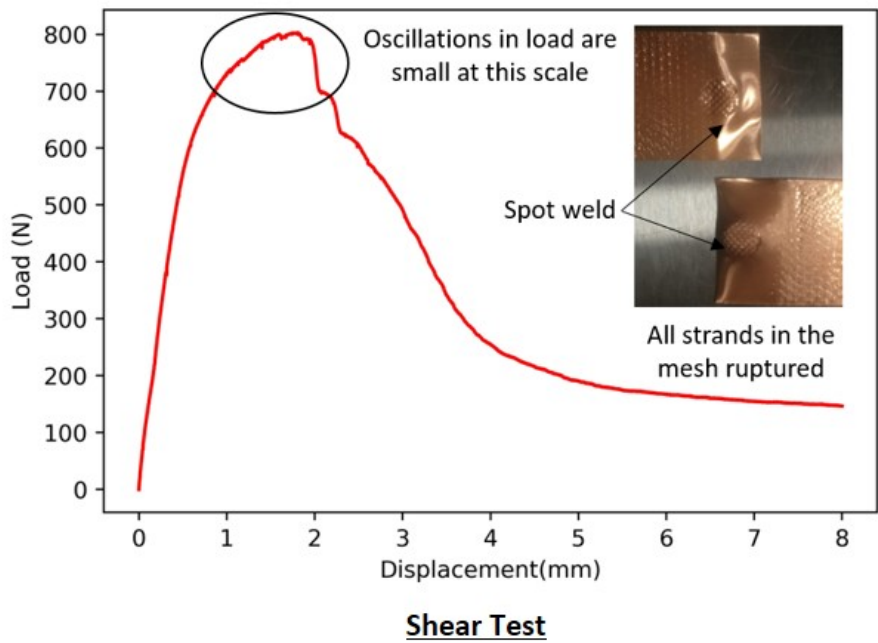
Figure 3.11: Example load curve of shear test of a USW joint
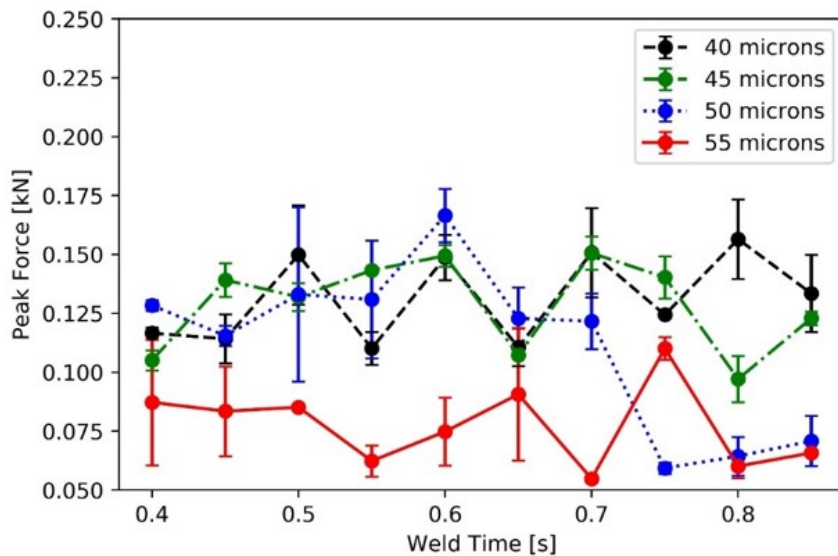
Figure 3.12: Results of peel tests of 10 mils thick, 8mm dia. USW joints using different weld parameters.
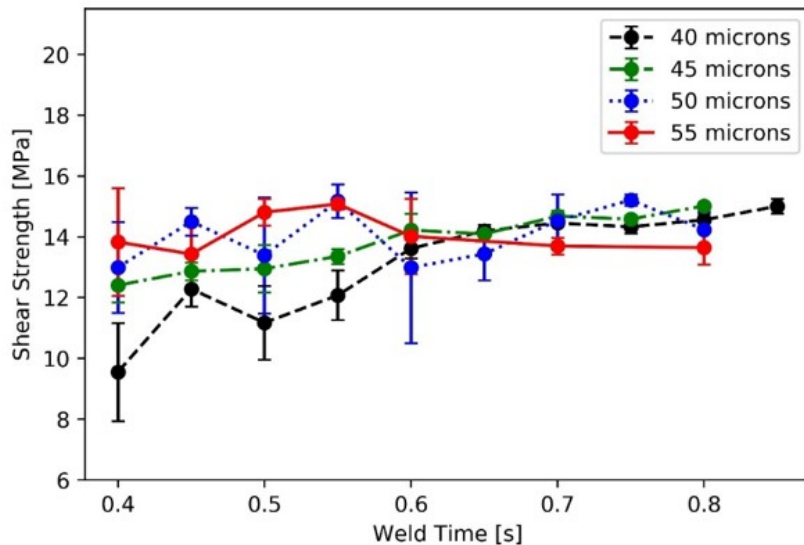
Figure 3.13: Results of peel tests of 10 mils, 8mm dia. USW joints using different weld parameters.
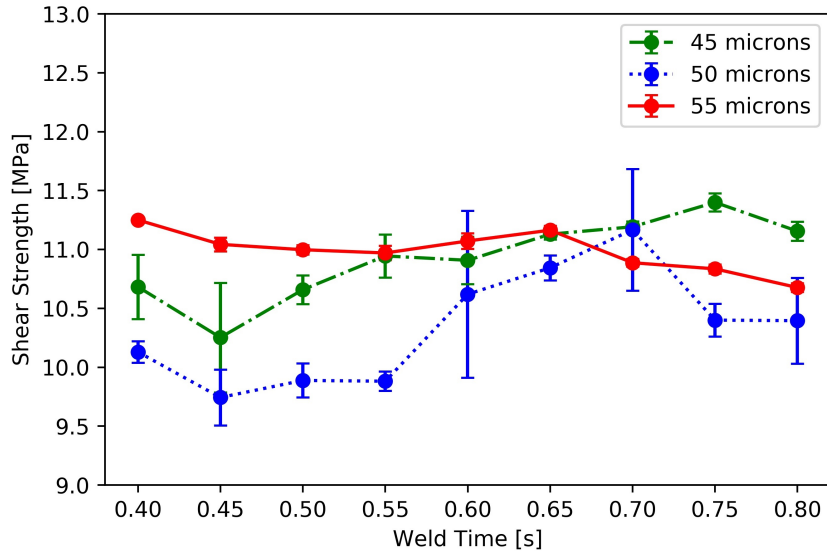
Figure 3.14: Results of peel tests of 8 mils, 8mm dia. USW joints using different weld parameters.

joints. Figure 3.13 shows peak shear strength data for USW joints between copper strips each with a thickness of 10 mils ($\sim 250\mu m$). We observe that the weld time does not have a significant effect on strength. However, higher weld amplitudes produce joints with higher shear strength with a peak at $50\mu m$. Figure 3.14 shows the results for similar tests on copper strips with a thickness of 8 mils ($\sim 200\mu m$). There is a marked decrease in average strengths, from 14 MPa at 10 mils ($\sim 250\mu m$) to 11 MPa at this lower thickness. Overall, weld amplitude of $50\mu m$ with a weld time of 0.6 s and higher thicknesses of copper are preferable for strong welds. To form tubes, the thickness is however limited due to the requirement for the strip to bend to form a curved surface.

CHAPTER 4

ROLL TO ROLL MANUFACTURING SETUP

4.1 Design of Setup

For producing the designs as depicted in previous sections, we created a helical tape laying setup. It is also dubbed as Roll to Roll (R2R) process because it consists of multiple webs of raw materials, which un-spool and then re-spool on a cylindrical mandrel in a particular fashion. The process is explained in this section. Refer to the appendix section for standard operational instructions.

The Lathe machine was the inspiration behind this setup. Figure 4.1 shows a perspective view of the full fabrication setup. Figures 4.2, 4.3 show the top view and side view respectively. It consists of four important parts, *viz.* Rotary system, Linear system, Syringe Pump system and Electronics (including Computer). We use motor control software developed by the Ferreira research group. Its main purpose is to control the motion of different motors in the system.

There are 2 linear axial stepper motors on the linear slides and 1 rotary stepper motor (NEMA 23 standard). The raw material housing is present one on each of the two linear systems. The rolls, also called spools, unroll from a specially designed spool holder. This spool holder has a passive pressuriser which helps in generating sufficient friction for normal
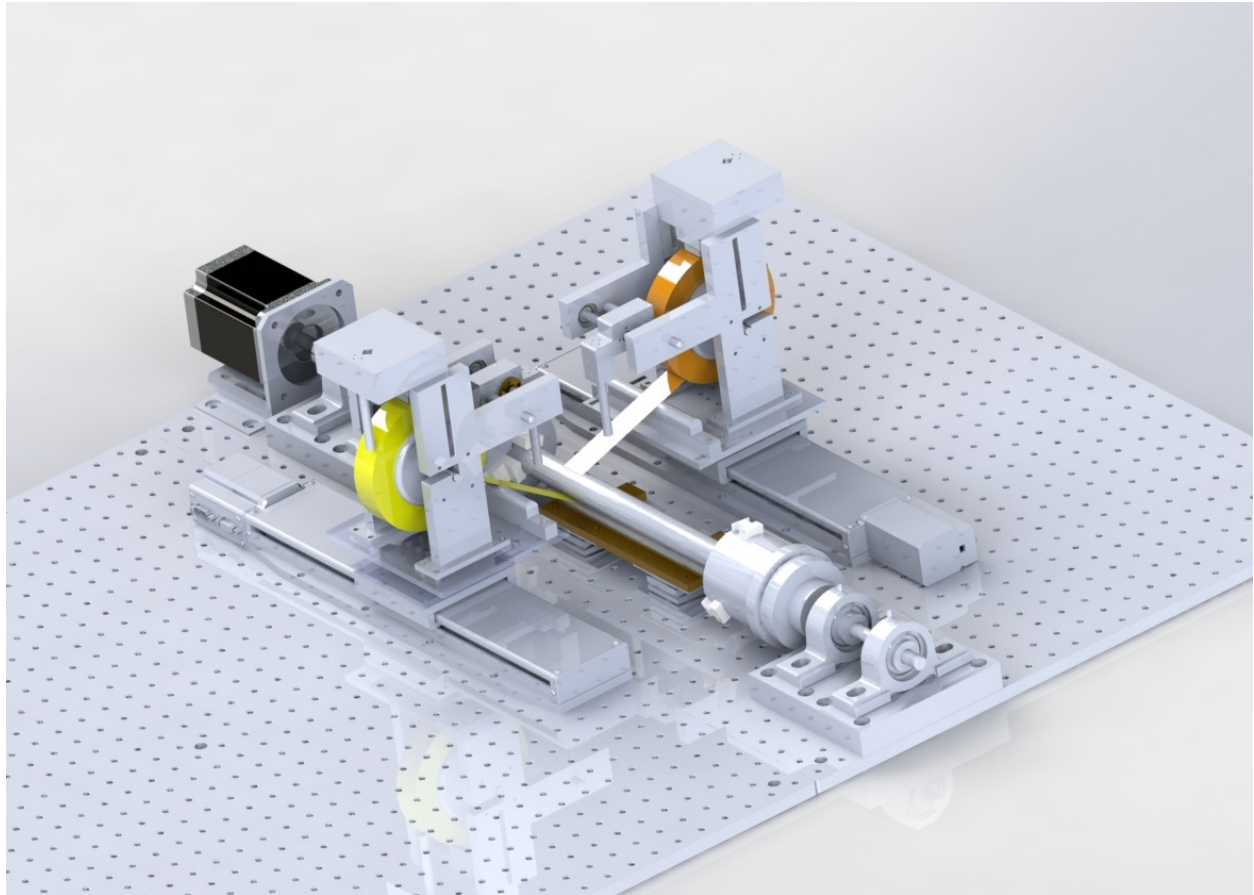
Figure 4.1: Perspective view of fabrication setup (Syringe Pumps and Electronics are not shown).
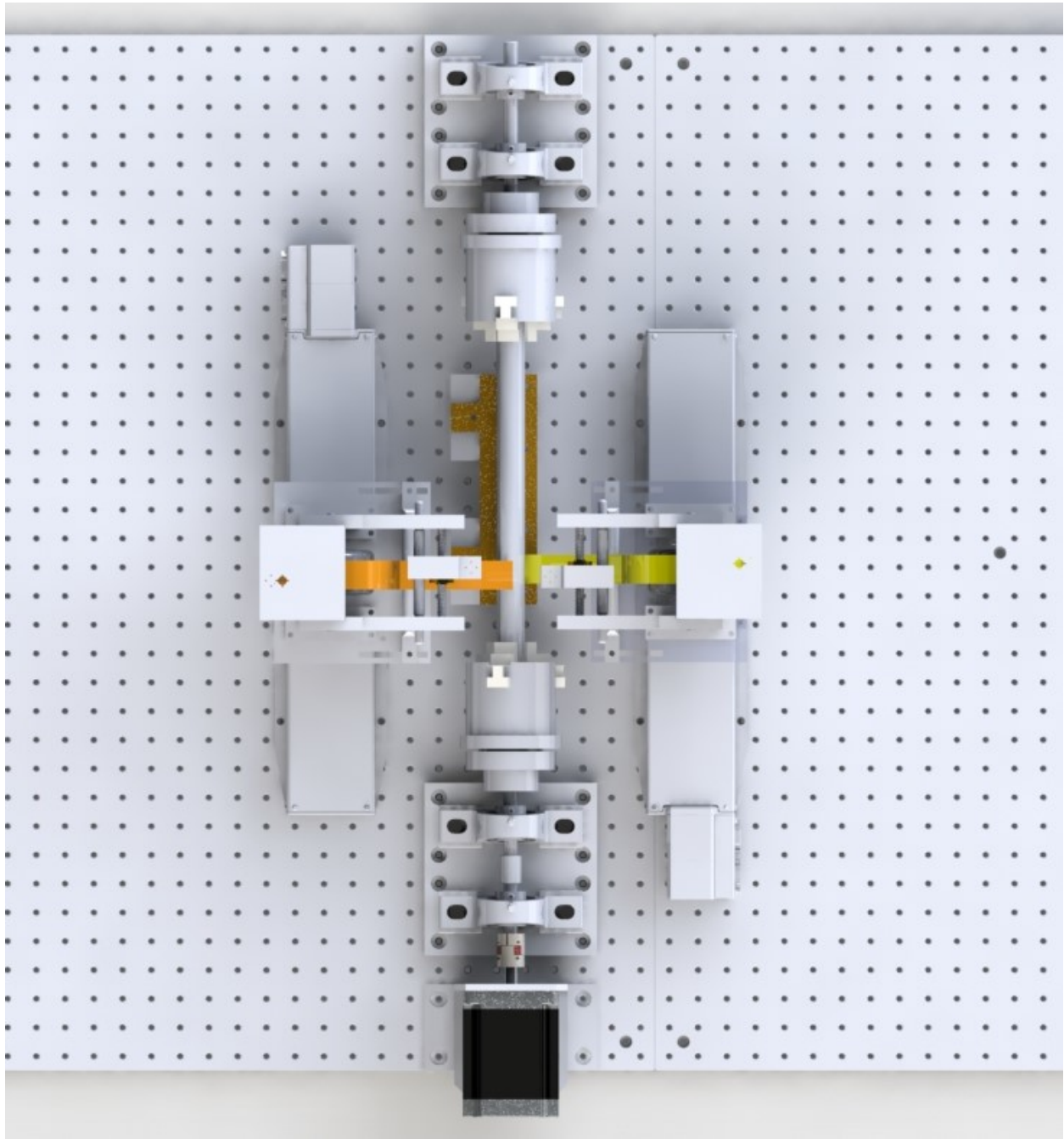
Figure 4.2: Top view of fabrication setup.
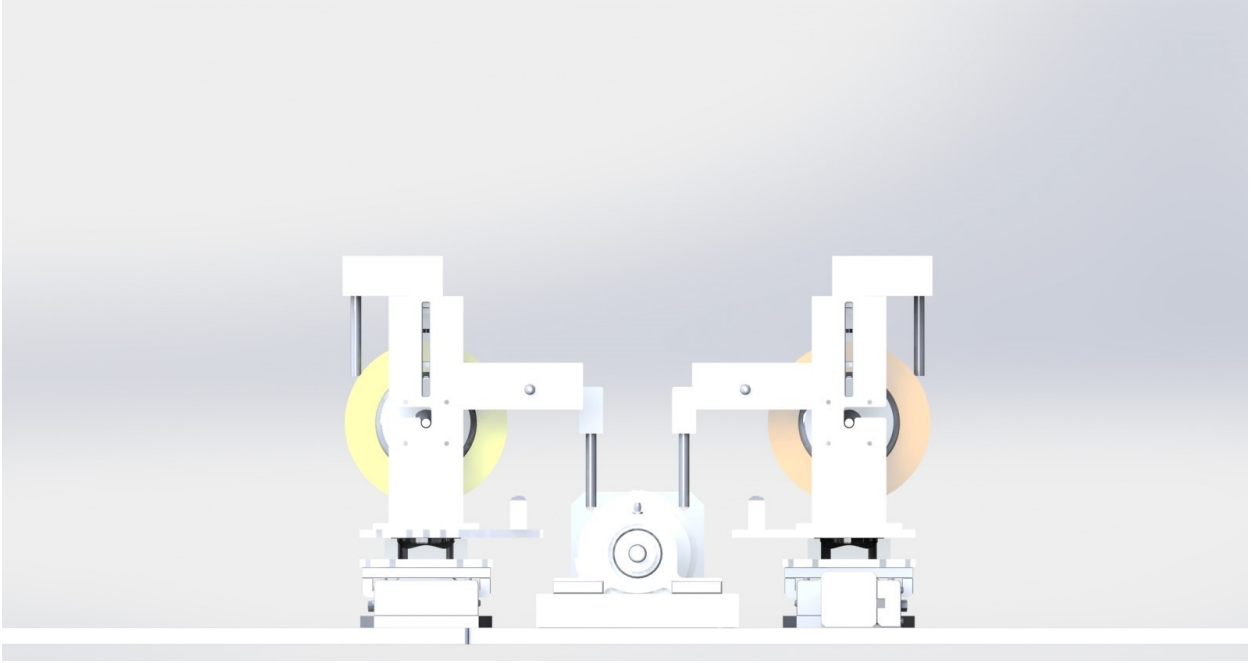
Figure 4.3: Side view of fabrication setup.

use.

The angle and speeds of unspooling are determined by calculating helical motion. **For a single tape**, equation 4.1 gives the approximate angle of helix which is formed by a conjoined rotary and linear motion. The Rotary motion of the tape, which unspools, is due to it's attachment to the mandrel. And the linear motion is due to the roll housing. For mechanics of both tape combined look further.

$$\theta = \arctan(\frac{l}{\pi dn}) \tag{4.1}$$

Here, l = length of the linear actuator (also the mandrel with pipe rolled onto it), d = outer diameter of the mandrel. Typical values of the angle are $\theta = 5 - 20°$. The real angle is close to this and may vary based on the thickness of the tape. Nonetheless, this is a good

estimate for design purposes. Refer to table 4.1 for candidate numbers. Note that this is for **one tape only**.

We are more interested in the overlap of the tapes of two different materials. Each of these feeds on to the mandrel at this helix angle. Number of turns (n) and initial tape offset (on the surface of the mandrel) are used to generate overlap length l_o. Equation 4.2 shows this relation mathematically

$$l_o = w - \frac{l}{n} \tag{4.2}$$

w is the width of the tape. n is the number of turns for length,l of mandrel or Figure 4.4

Table 4.1: Helix angle & overlap length for l = 200mm and w = 25.4mm (1 in.)

Number of turns (n)	Angle (θ)	Overlap length (l_o)
10	14.1°	5 mm
15	9.5°	11.67 mm
20	7.15°	15 mm

shows one of the initial prototypes of a self rolled tube. By this we mean that a single tape was rolled onto itself. This is controlled by the equation shown above. By extension, the speeds of the two motions are linearly related by the following equation **??**. Note that helix angle should remain constant for the duration of motion.

$$\frac{dl}{dt} = \pi d \ arctan(\theta) \frac{dn}{dt} \tag{4.3}$$

For **dual tapes**, the relation between approximate angle and overlap length is given by the following equation 4.4. Note that each tape unspools from about symmetrically located (on the opposite side of the mandrel) linear tape dispensers. Also, they are initially offset on the axial direction by l_0.

Figure 4.4: Self rolled copper tape with acrylic adhesive on tape. Approximate dimensions are w = 25.4 mm, l = 200 mm, d = 25.4 mm, $\theta = 14°$, $l_0 = 5.4mm$

$$l_0 = \frac{1}{2}[w_1 + w_2 - \pi d \ tan(\theta)] \tag{4.4}$$

Here 'w' represents the width of individual tapes. An example: 1 wide Copper and 1 wide Kapton tapes produce 0.47 overlap for $\theta = 10°$. It is recommended that you use tapes of equal width. Otherwise, there may be problems during overlap.

4.2 Parts and Modularity

The real setup built by us is located in the Sinha lab at UIUC, as shown in figure 4.5.

As mentioned before, the fabrication setup consists of various subsystems. Figures in the previous subsection showed only Rotary setup and Linear setup. All the four subsystems are individually replaceable without modifying the other subsystems substantially. Figures
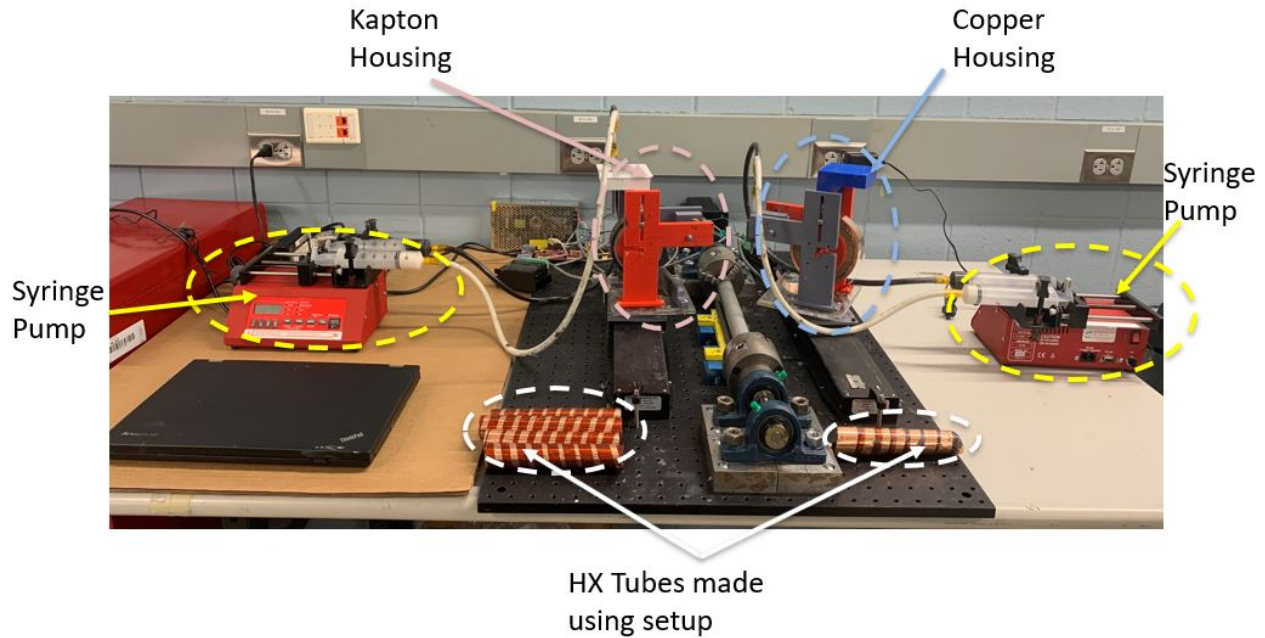
Figure 4.5: Side view of the actual fabrication setup at UIUC

4.6, 4.7 and 4.8 show the perspective view, top view and side view of the Rotary system in more detail.

Figures 4.9, 4.10 and 4.11 show the perspective view, top view and side view of the Linear system in more detail.

The web holder for the raw material (Kapton or Copper) has been specifically designed to ensure smooth rotation and holds the 3 inch web via an interference fit. Figure 4.12 shows this part in more detail. Special care has been taken to design the mechanisms intended to move the adhesive mixer tube into a position for dispensing mixed adhesive onto the material film.

The syringe pumps are connected to the Linear setup as shown in the following schematic in Figure 4.13.

A presser for mandrel is present to apply pressure when rolling is in process. This addi-
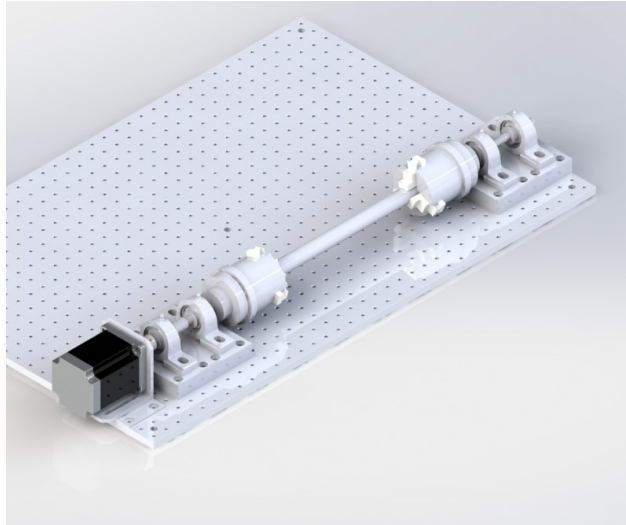
Figure 4.6: Perspective view of Rotary setup.
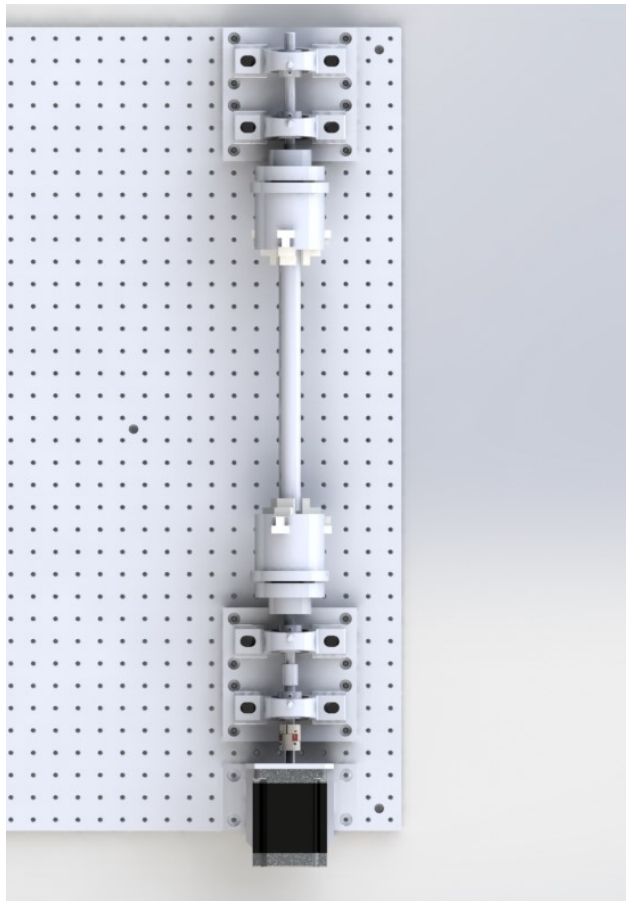
Figure 4.7: Top view of Rotary setup.
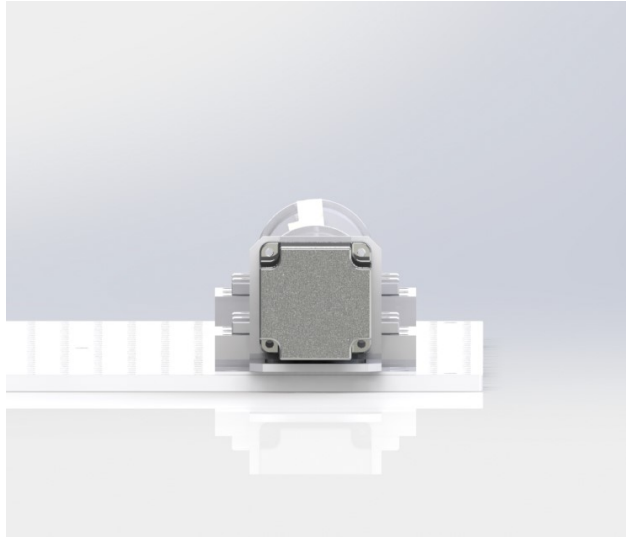
Figure 4.8: Side view of Rotary setup.
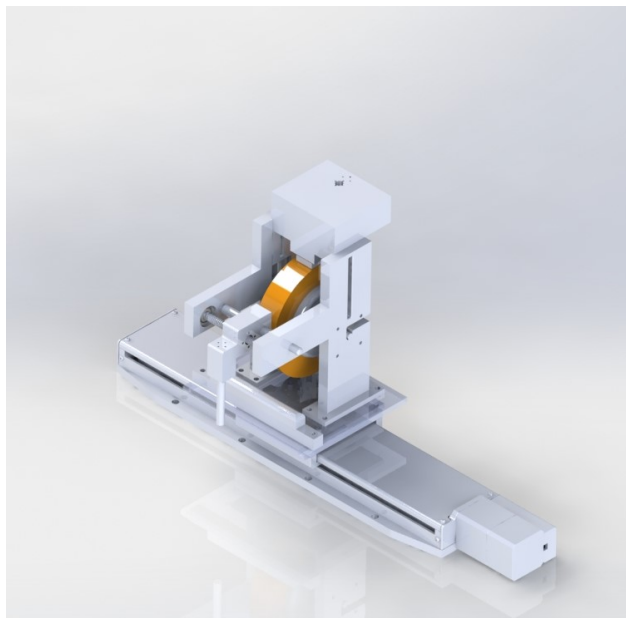
Figure 4.9: Perspective view of Rotary setup.
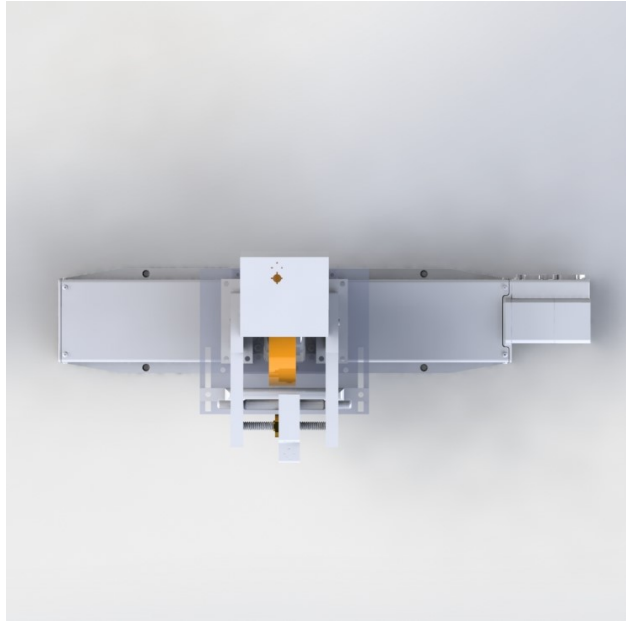
Figure 4.10: Top view of Rotary setup.
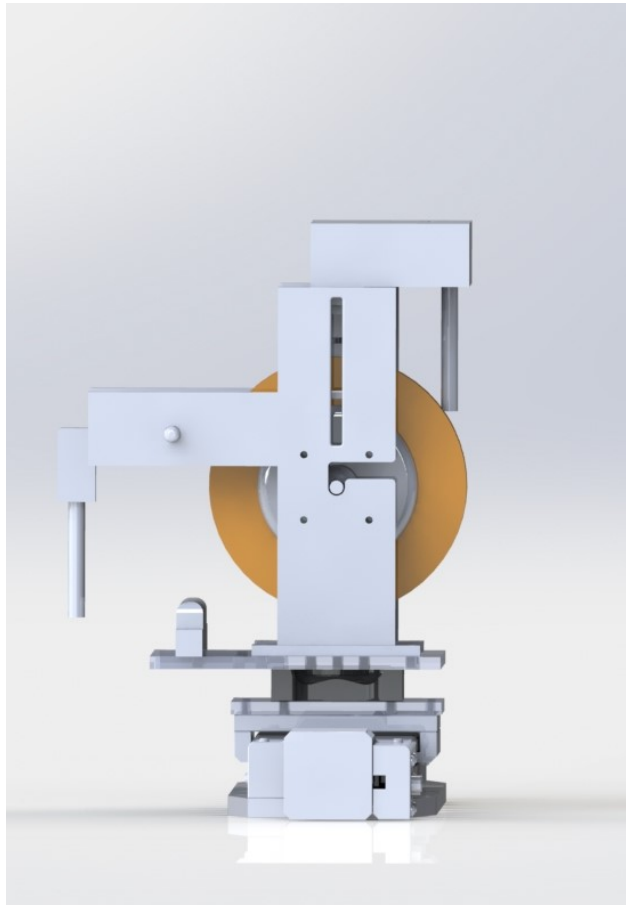
Figure 4.11: Side view of Rotary setup.
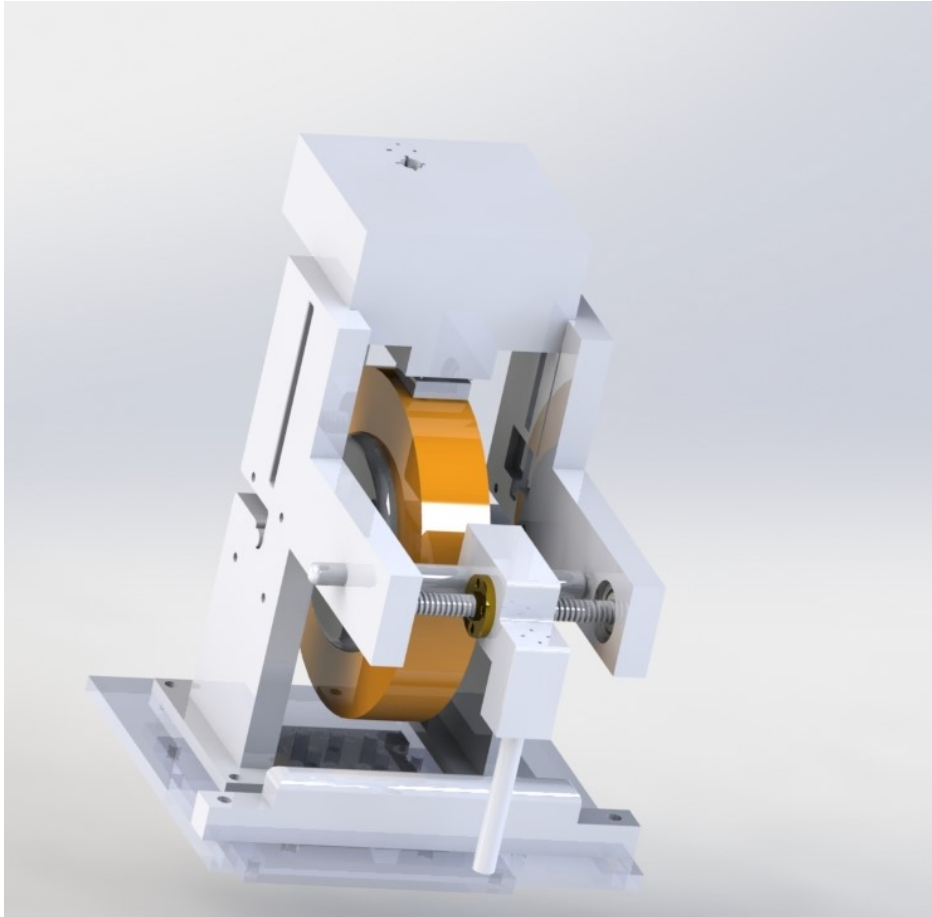
Figure 4.12: Perspective view of web holder and parts of adhesive dispenser.
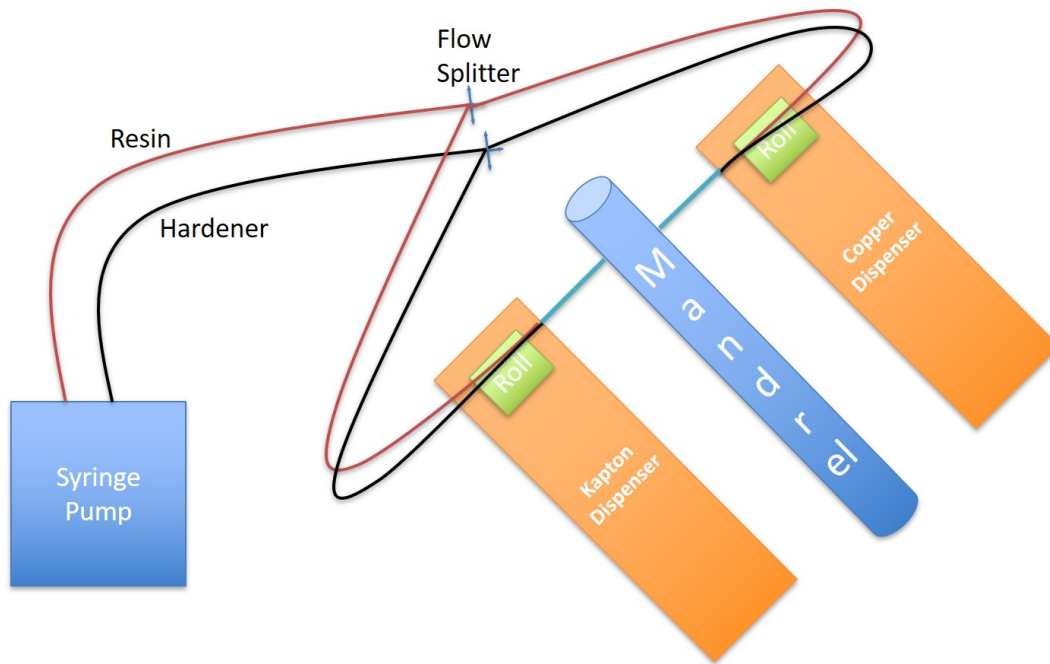
Figure 4.13: Connecting syringe pump to the dispenser setups.

tional metal roller is necessary until the set time of adhesives is reached. It can be removed afterward. Figure 4.14 show the schematics for this part. Height adjustor is added to ensure there is sufficient contact pressure between rolled tapes and dispensed adhesive.
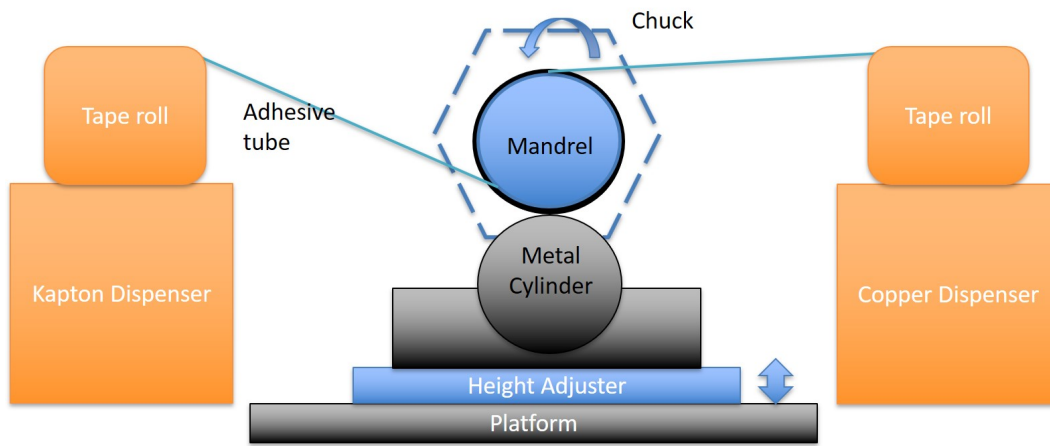
Figure 4.14: Presser present underneath the collapsible mandrel to ensure contact between films and adhesives.

CHAPTER 5

PERFORMANCE OF HX

5.1 Wind Tunnel Apparatus

Performance of the tubes has been tested in wind tunnel present in MechSE department. The schematics of the wind tunnel are shown in the figures 5.1 and 5.2. This is a complicated system with many subsystems. It is nearly 28 years old at the time of this writing. We attempted to incorporate our system as smoothly as possible. It mainly consists of an air heater, blower, flow straightener, test section, and a fluid chiller. It is also retro-fitted with thermocouples, flow control , and measurement meters. A National Instruments based LabView software code is used to perform the experiments and capture data recorded at different measuring devices.

5.2 Design of HX with Hybrid Tubes

We explored multiple connection options for R2R tubes. They are connected in series to ensure temperature difference is measurable using RTD temperature sensors placed at the ends of the piping. Figures 5.3, 5.4 and 5.5 show our designs using different end fittings and placement of tubes. Design 1 contains flexible tubing. PVC pipes used in design 2 for improved tolerances. Design 3 uses bellow tubes to allow for easy connections and
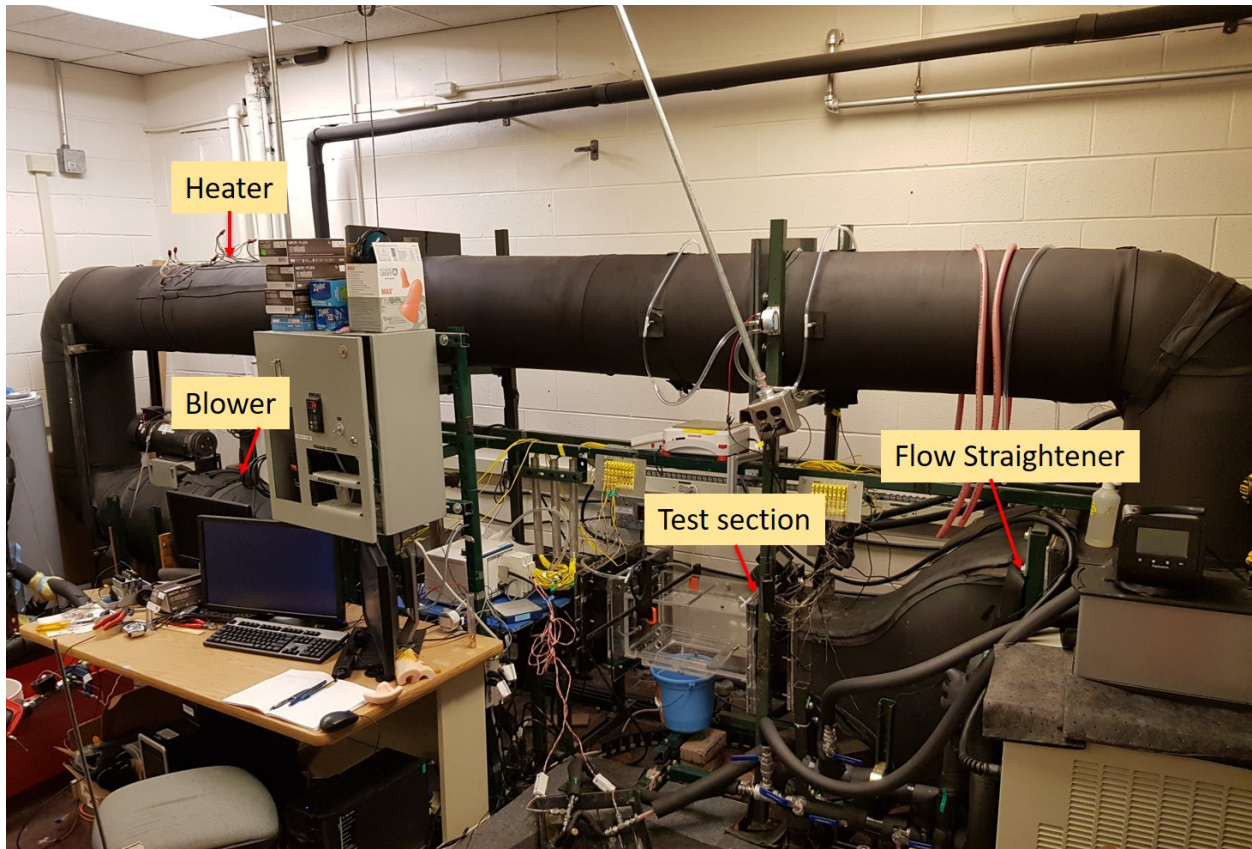
Figure 5.1: Wind Tunnel Apparatus located in MechSE UIUC (Chiller is not shown). (Credits: Energy Transport Research Lab, UIUC)
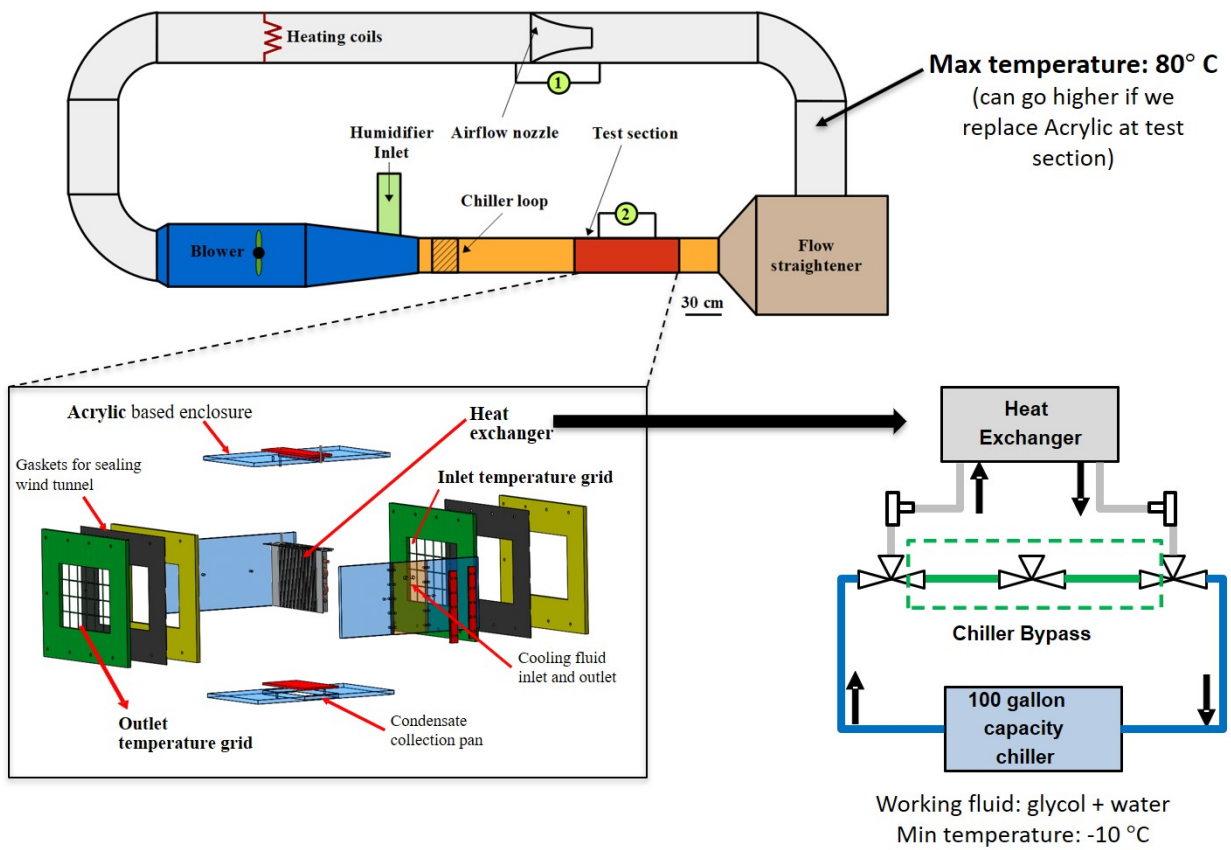
Figure 5.2: Wind Tunnel Schematics (Credits: Energy Transport Research Lab, UIUC)
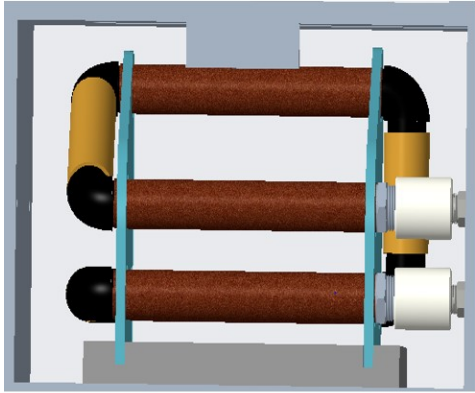
Figure 1: Back view for HX Design 1
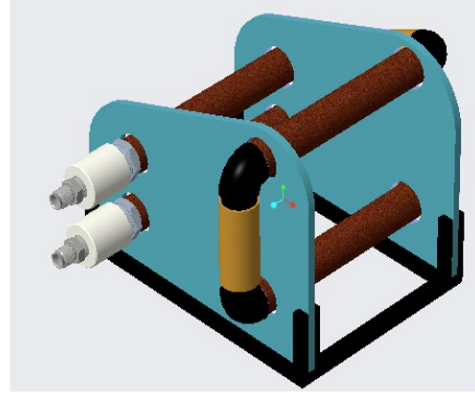
Figure 2: Standard Orientation for HX Design 1
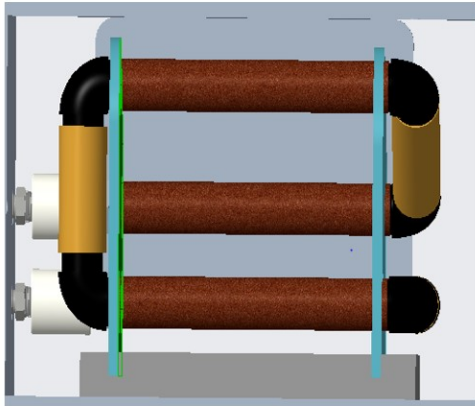
Figure 3: Front view for HX Design 1
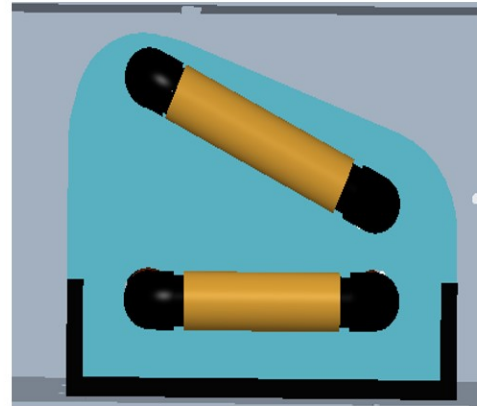
Figure 4: Side view for HX Design 1

Figure 5.3: Heat Exchanger design 1 consists of flexible plastic tubing

modularity. Based on our experiments, we found that design 2 is good for reproducibility. Design 1 was prone to leakage and design 3 was not feasible due to size constraints.

Hybrid tubes were arranged in a series linkage (with respect to fluid flow) to increase the residence time of the cold fluid inside the test section of wind tunnel. This has been done to ensure that the temperature rise of cold fluid observed to be greater than the least count of thermocouples.
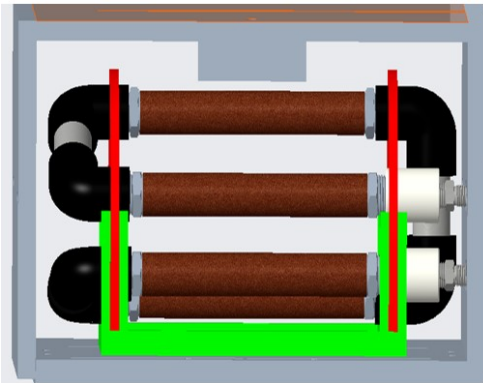
Figure 1: Back view for HX Design 2
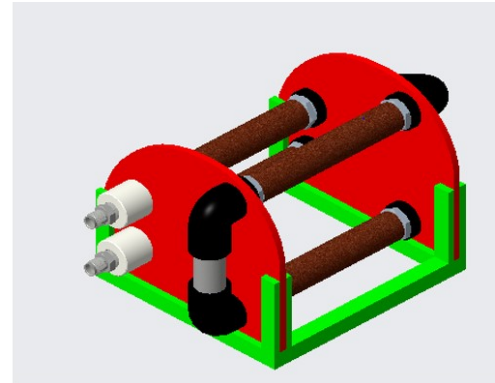
Figure 2: Standard Orientation for HX Design 2
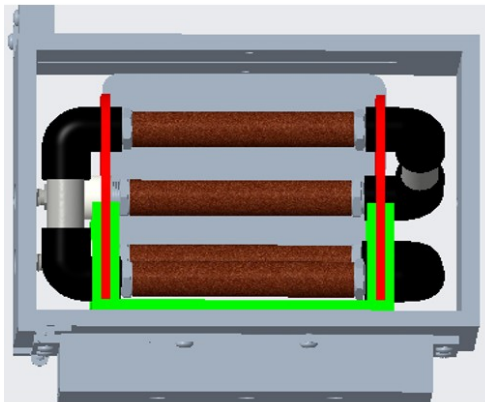
Figure 3: Front view for HX Design 2
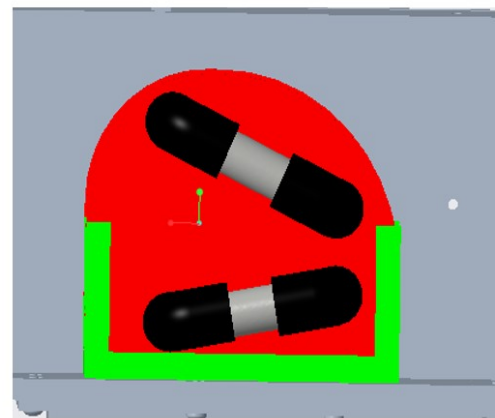
Figure 4: Side view for HX Design 2

Figure 5.4: Heat Exchanger design 2 consists of rigid plastic tubes and fittings
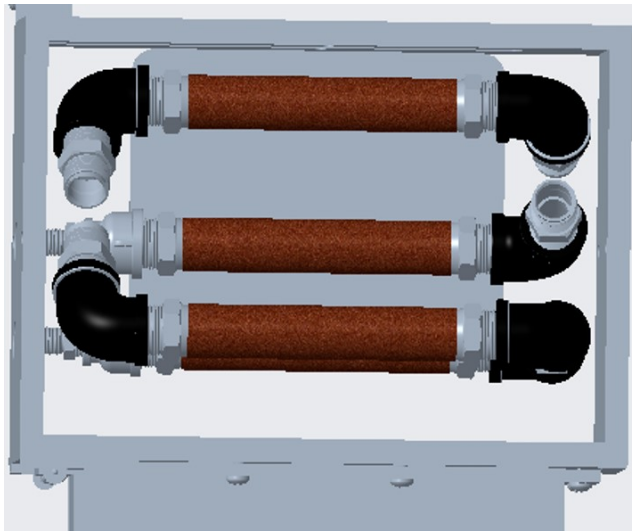
Figure 1: Front view for HX Design 3
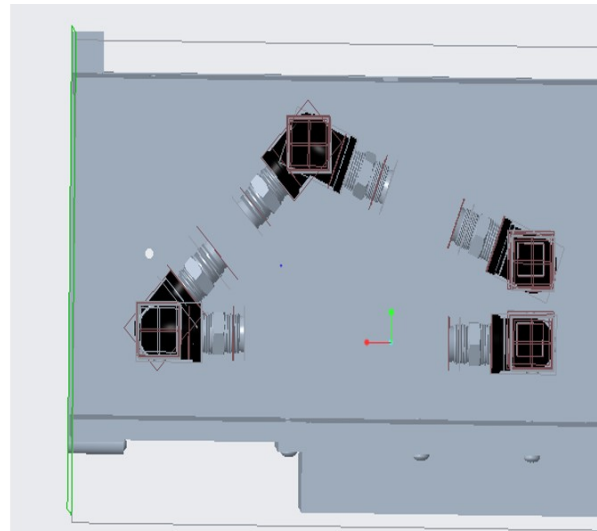
Figure 2: Side view for HX Design 3

Figure 5.5: Heat Exchanger design 3 consists of flexible bellows tubing made of metal

Figure 5.6: Temperature variation in a 4 tube, all Kapton, cross flow configuration.

5.3 Wind Tunnel Characteristics

To identify the capabilities of the wind tunnel, we performed different tests as shown in the following figures. To understand the variation of temperatures and time constants involved in this process, a variety of tests were performed. Details are specified in each of the figures 5.6, 5.7 and 5.8. These plots differ in terms of experimental conditions. They also help clarify the capabilities of the wind tunnel system for future testing.

Temperatures and Flow rates were juxtaposed on the same plots in figures 5.9,5.10 and 5.11. This shows inplot comparison of these quantities.

Figure 5.7: Temperature variation in a 4 tube, all Kapton, cross flow configuration (different conditions).
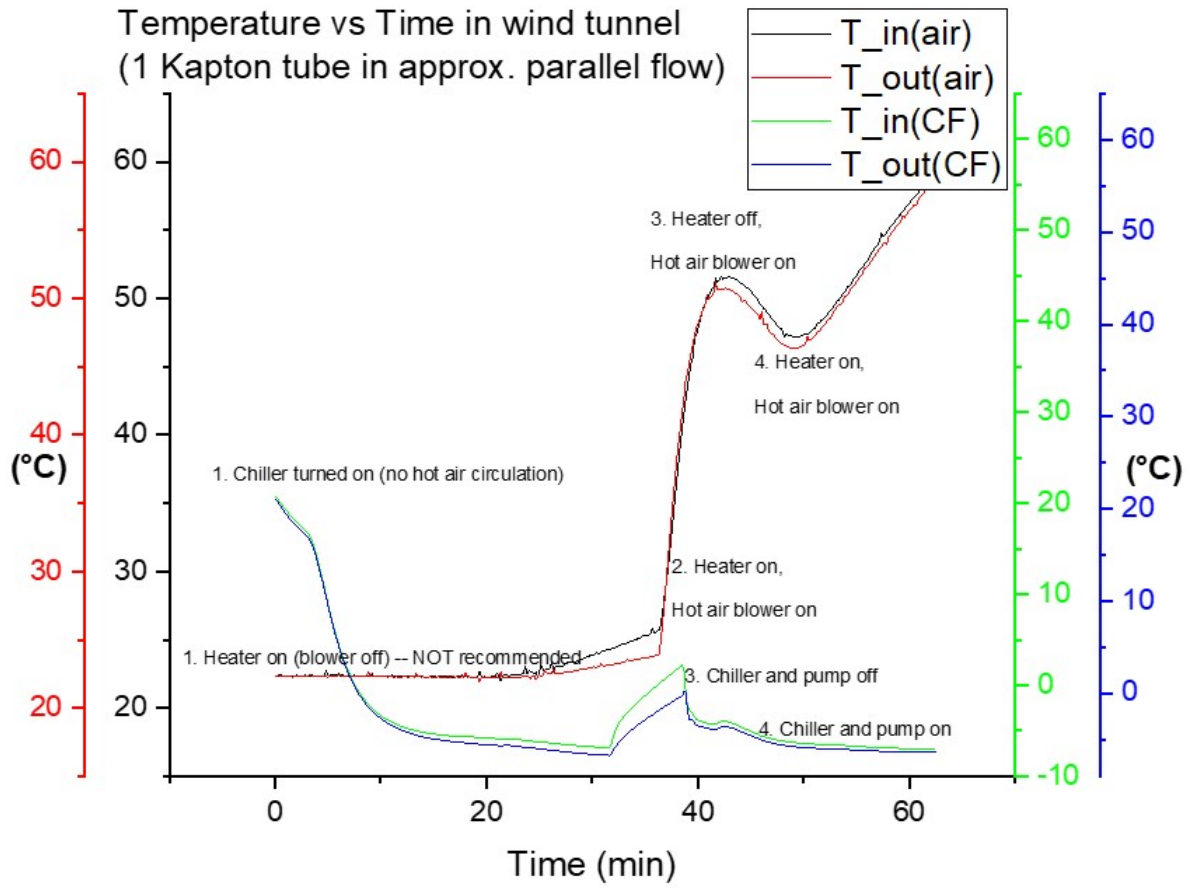
Figure 5.8: Temperature variation in a 1 tube, all Kapton, near parallel flow configuration.
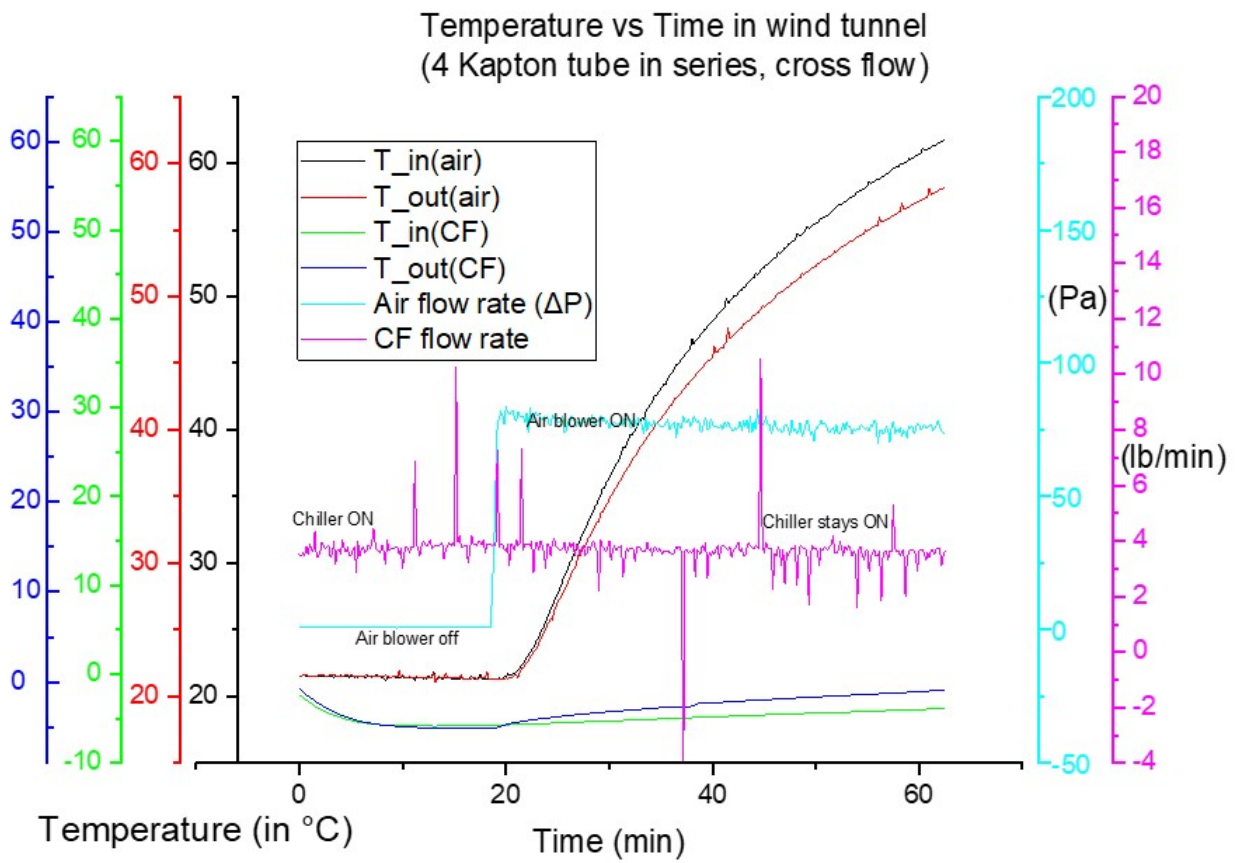
Figure 5.9: Includes flow rates in addition to temperatures, refer to 5.6
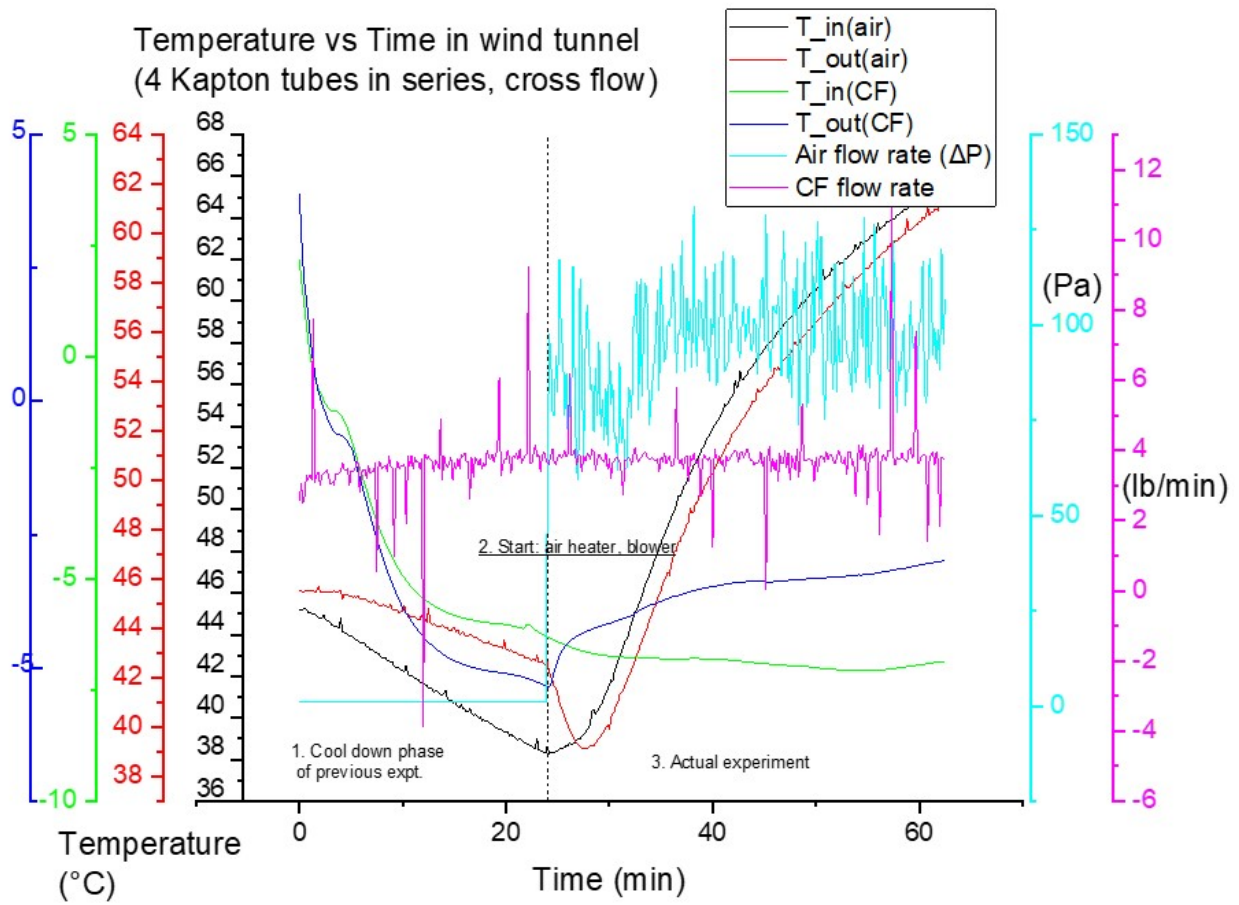
Figure 5.10: Includes flow rates in addition to temperatures, refer to 5.7
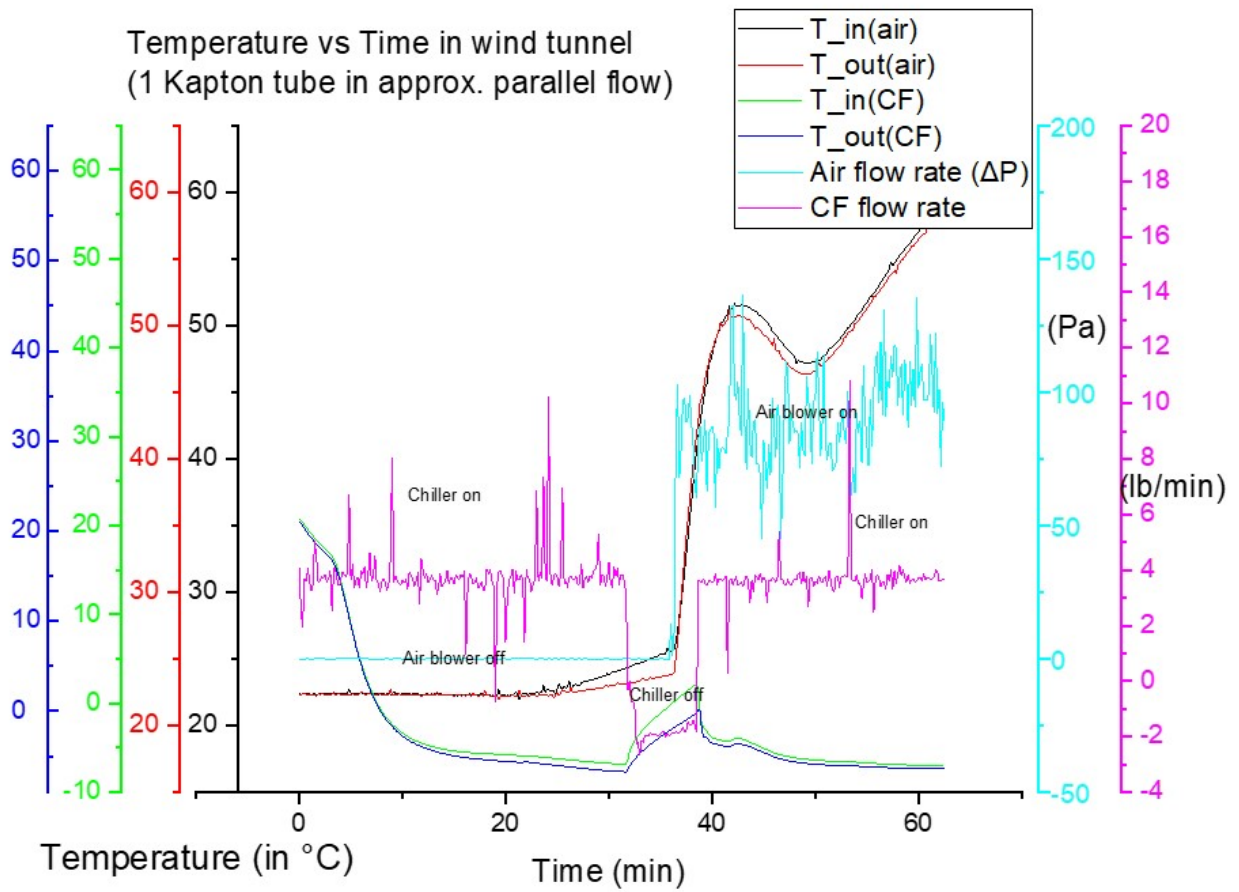
Figure 5.11: Includes flow rates in addition to temperatures, refer to 5.8
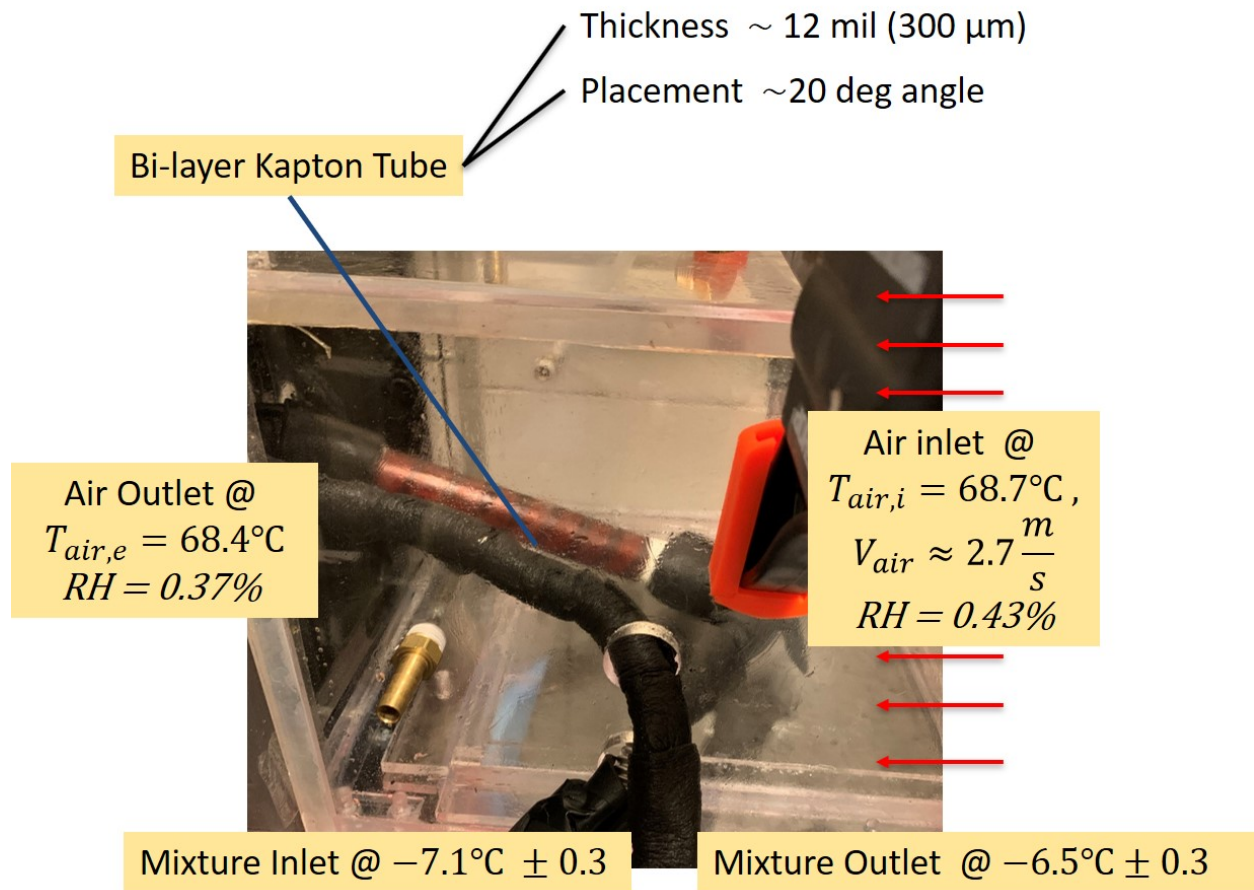
Figure 5.12: Single bi-layer Kapton tube in nearly parallel flow. Numbers in the inset show flow properties for a specific test.

5.4 Test Results

Taking into account physical constraints, only specific tests, as shown in the following paragraphs, were performed to assess the performance of these Heat Exchangers.

Test1 (Single bi-layer Kapton Tube): First test consists of a bi-layer Kapton tube made using silicone adhesive as the joining method. The total tube wall thickness is 300 m. Length of the tube is 7 and diameter is 1. It was placed at an angle of 20 to the base of test section. Fluid flow can be summarised as a near parallel flow configuration. Figure 5.12 shows this tube in test section.
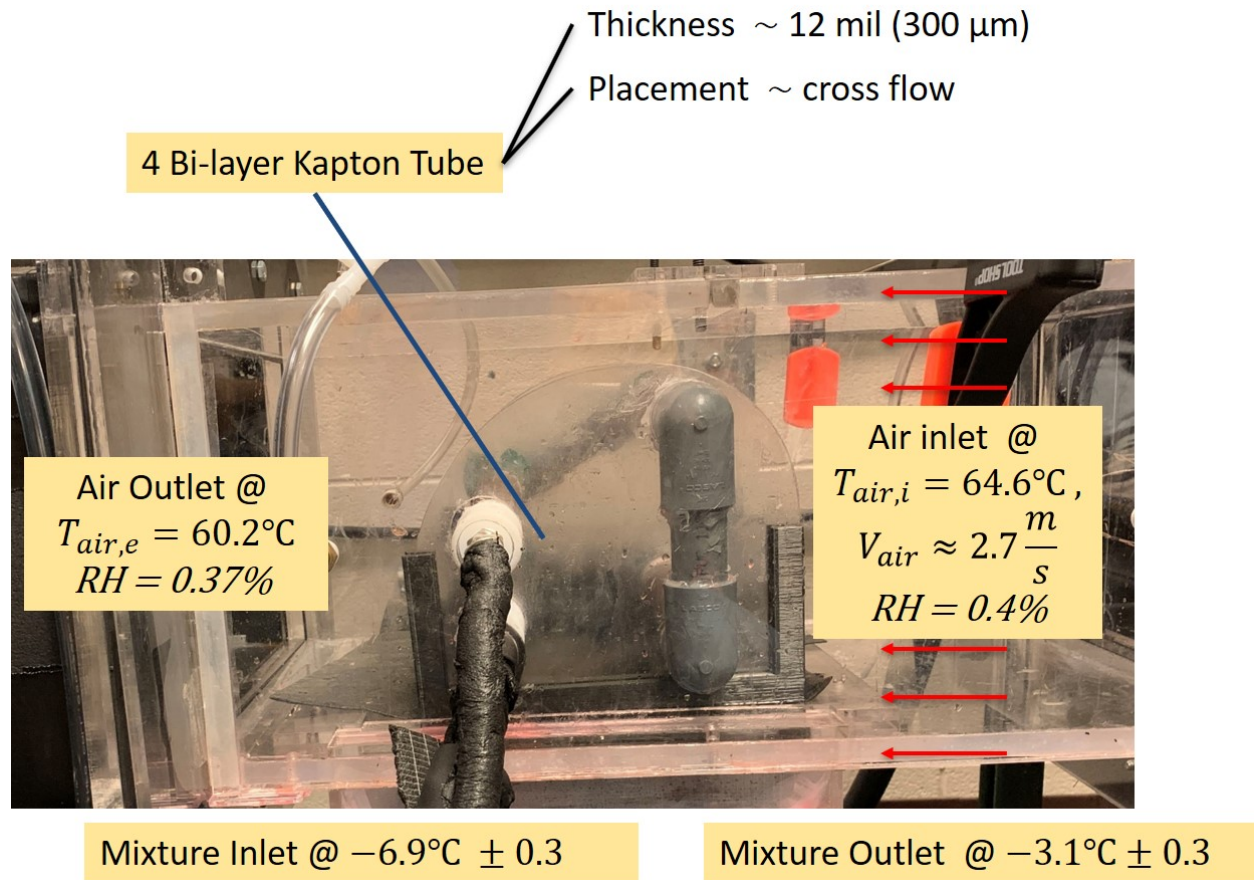
Figure 5.13: Design 2 with 4 bi-layer Kapton tubes connected in series with heat transfer in cross flow. Numbers in the inset show properties for a specific test.

Test2 (Design 2, PVC fittings, 4 bi-layer Kapton tubes): This test consists of a four bi-layer Kapton tubes connected in a series flow configuration. Heat transfer across hot air and cold fluid mixture happens in a cross-flow mode. They are connected at the ends by PVC tube fittings. Tubes are approximately 6 inch in length (individual), diameter of each tube is 1 inch. Thickness of the wall layer is about 300 m. Figure 5.13 shows this HX test setup inside test section.

Results of these two tests are shown in the tables 5.1 and 5.2. Simple calculations using basic heat transfer equation estimates the net heat recovered by these two tests to be **test1:**

Table 5.1: Test1: HX heat recovery in Windtunnel

Fluid	Temp	Before heating	After heating (1hr later)
Air	T_{in}	22.46°C, RH = 46.5%	68.7 °C, RH = 0.43%
	T_{out}	22.27°C, RH = 47.3%	68.4 °C, RH = 0.37%
58.5% V/V Ethylene Glycol - Water Mixture	T_{in}	−6.8°C	−7.1°C
	T_{out}	−6.7°C, $\delta T = 0.1$°C	−6.5°C, $\delta T = 0.6$°C

Table 5.2: Test2: HX heat recovery in Windtunnel

Fluid	Temp	Before heating	After heating (1hr later)
Air	T_{in}	43.2°C, RH = 6.1%	64.6 °C, RH = 0.4%
	T_{out}	39.4°C, RH = 5.8%	60.2 °C, RH = 0.37%
58.5% V/V Ethylene Glycol - Water Mixture	T_{in}	−6.1°C	−6.9°C
	T_{out}	−5.1°C, $\delta T = 1$°C	−3.1°C, $\delta T = 3.8$°C

55W/tube (about 306 W/m/tube), **test2: 86W/tube (about 478 W/m/tube)**. In both cases, the heat recovered is nearly equal to or greater than **10%** heat recovery which requires 310 W/m in this case.

$$\dot{Q} = \dot{m} * C_p * \Delta T \qquad (5.1)$$

where $\dot{Q}$ is the heat energy, $\dot{m}$ is the mass flow rate of cold fluid, C_p is the specific heat capacity of cold fluid. δT is the temperature difference the bulk of between hold and cold fluid. Ethylene Glycol mixture is the cold fluid in this case. Air is the hot fluid. RH is the relative humidity of air.

5.4.1   Limitations

The preceding analysis shows a potential recovery of 86 W watts per tube. From a heat transfer perspective, we expect the heat recovery to be limited by air side convection coeffi-

cient. It can be proved as shown in the following analysis.

The overall heat transfer coefficient (U_{eff}) of a pipe in a flow scenario is given by eq 5.2.

$$\frac{1}{U_{eff}} = \frac{1}{h_i} + \frac{1}{h_o} + \frac{t}{k} \tag{5.2}$$

In a more particular application to a cylindrical geometry, we can use the following equation 5.3 for analysis. where h_i and h_o are internal and external convection heat transfer coefficients. t is the thickness of the wall of heat exchanger. k_{wall} is its effective thermal conductivity. A_i, A_o, A_{eff} represent the heat transfer surface areas. The effective surface area is a mean of the earlier two. r_i is the internal radius of the tube.

$$U_{eff} * A_{eff} = \frac{1}{\cancelto{0}{\frac{1}{h_i * A_i}} + \frac{1}{h_o * A_o} + \frac{\ln \frac{r_i + t_{wall}}{r_i}}{k_{wall} * 2\pi\ l}} \tag{5.3}$$

In a typical situation, we have numerical values of about $h_i \gtrsim 200\ W/m^2K$ and $h_o \approx 10W/m^2K$. Inner fluid (water) is at temperatures of about $23°C$ and a flow rate of 0.1 kg/sec. Outer fluid (air) is at about $150°C$ and flows at a mean speed of 3 m/sec or about $5\ m^3/sec$. As shown in equation 5.3, by numerical comparison, waterside term goes to zero and now the effective h is limited by airside. Figure 5.14 shows the variation in pictorial format [11, 12] at different fouling conditions. To look at the general trend of saturation in U is enough for the sake of this argument.

Due to unavailability of raw materials in higher thicknesses in required format, we performed experiments with low thicknesses of 10 mils ($\approx 150\mu m$. Hence we observed superior thermal conductivity even without the addition of copper. But for actual industrial applica-

$$U = \cfrac{1}{\cfrac{1}{h_{flue} * A_o} + \cfrac{\ln\dfrac{r_i + t_{wall}}{r_i}}{k_{wall} * 2\pi L} + \cfrac{1}{h_{water} * A_i}}$$

For t = 2.5mm
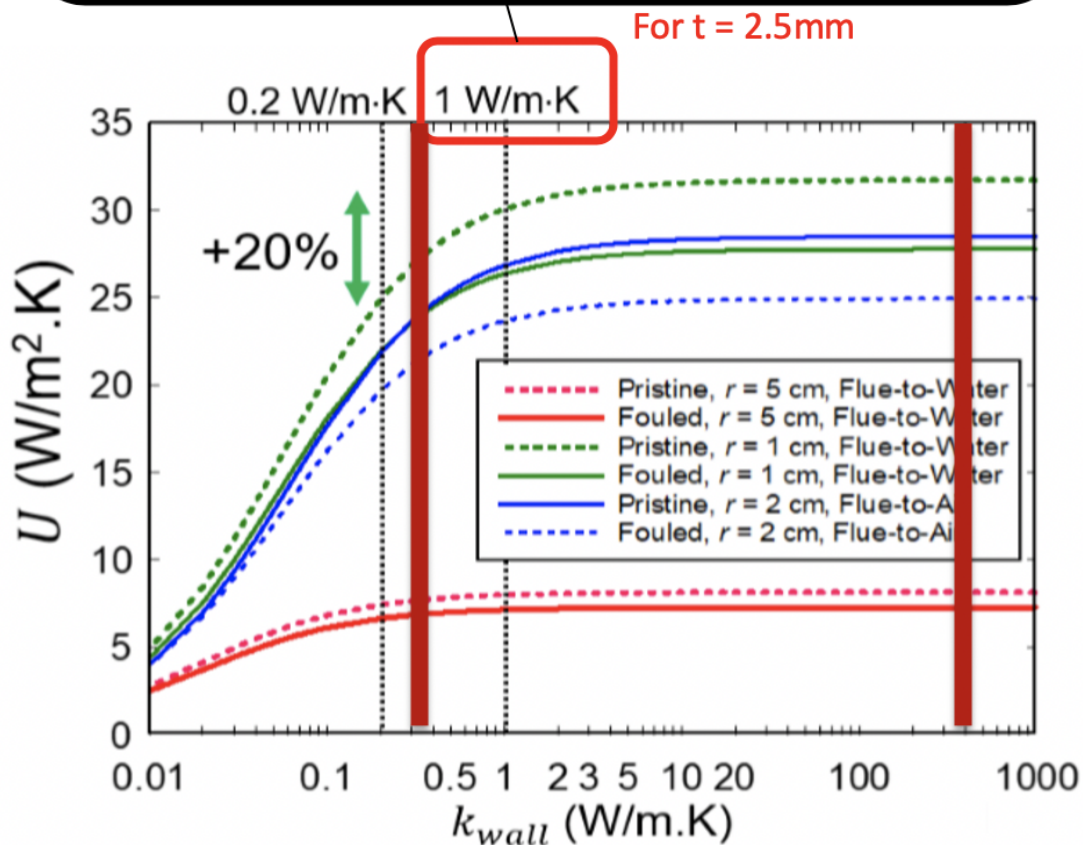
Figure 5.14: Overall U across a certain cross-flow HX. Improvement of U is limited by the ratio of thickness, t_{wall} and thermal conductivity K_{wall}

tions, it is recommended to use thicker pipes for better mechanical stability [11]. This will

mandate the use of roll to roll processed Copper-Kapton HX tubes as observed in figures

2.4 and 5.14

CHAPTER 6

SUMMARY & CONCLUSIONS

6.1 Summary

In this thesis work, the primary focus was on developing a design and manufacturing system for producing a novel heat exchanger using metals and polymers. We faced many issues trying to bring the best of both worlds. Next paragraphs succinctly capture particular issues and solutions.

6.1.1 Materials and Joining

Since most of this work was built upon new ideas, we stumbled at multiple points during this project. Firstly, choosing a suitable material for achieving optimal heat transfer at $150 - 200°$ was a tough challenge. Most plastic materials decompose below the boiling point of water. Very few commercial plastics stay mechanically rigid at higher temperatures. The available ones are very expensive and do not cut the cost metrics except on large scales. So, we chose Kapton as a viable polymeric solution. And Copper was the metal of choice from the beginning for its superior thermal and mechanical properties albeit costs on the higher side.

After choosing the polymer our next step was choosing a suitable joining mechanism to

create a permanent, sealing bond between the metal and polymer. We explored adhesives, ultrasonic welding and lasers (partially) as candidates for joining. After experimentation, we went ahead with epoxy adhesives because of its ease of integration into a bigger scale manufacturing setup.

6.1.2 Manufacturing System

To achieve the helical geometry of our HX designs, we took inspiration from the lathe machine. We reimagined a joining process wherein there are linear setups and rotary setups to simulate X (linear) directional motion and circular motion. In conjunction, these two motions create a helix. To achieve this we purchased linear slides and re-purposed it to suit this project. Linear slides held a housing setup for material tape rolls. Rotary setup holds a collapsible mandrel in chucks. The collapsible mandrel is necessary for removal of the manufactured HX tube.

We encountered many issues, which we solved after comprehensive brainstorming. Tape slippage during feeding occurred due to play in the cylinder. It was solved by a torsional damper. Mandrel design was modified several times to collapse easily at the end of HX tape laying process. Irregular increase in overlap length was solved by selectively controlling the azimuthal angle of tape housing (Z-axis is perpendicular to the base plate). Synchronizing stepper motors also improved the efficiency of rolling process.

We developed an adhesive dispensing mechanism by using dual syringe pumps and controlling the push rates. Both linear slides were connected to one syringe pump. This can be further improved as explained in the next section.

6.1.3 Testing in Wind Tunnel

We performed preliminary testing in the wind tunnel using self-rolled Kapton tubes and reported the results. For this purpose, we built a heat exchanger module which holds at least four rolled HX tubes in series (with regards to fluid flow). Tests on Copper only tubes were performed but tests were inconclusive owing to the poor material thickness. We faced issues in the form of poor handleability of tubes (due to extreme thinness) and water leakage. We performed experiments with every care to ensure good results. Silicone helped in sealing end joints. Using multiple layered HX tubes improved its handleability by many folds. In the end, preliminary testing on multi walled Kapton tubes showed a potential heat recovery of 86W/tube of heat recovery. This number is satisfactory. More tests can be conducted in the future.

6.1.4 Closure

In summary, we worked on producing novel hybrid metal polymer heat exchangers joined using adhesives. We explored other joining techniques as well. We created a roll to roll process inspired manufacturing method to realize these hybrid heat exchangers tubes. These tubes were arranged in different configurations and tested in a wind tunnel. Heat recovery from this heat exchanger was satisfactory ($\gtrapprox$ 10% heat recovery).

6.2 Future Work

This work lays stepping stones for testing tape rolled hybrid heat exchangers. Improvements can be made in the tape-laying and bonding accuracy of the current manufacturing system.

Further systematic testing can be performed to fully specify the performance of the hybrid HX. Future work is needed to further establish the designs and improve the adhesive dispensing via the syringe pump. Further improvement in heat transfer performance can be achieved by enhancing fluid side properties.

6.2.1   On Tape Materials

Detailed experimentation was done only between Copper and Kapton. It would be interesting to see the thermomechanical performance of joints formed between other metals and polymers.

For example, Aluminum is a strong contender as a replacement for copper. But it suffers from poorer thermal conductivity. Because it costs much less than Copper, the overall purpose of replacing sections of it with polymer is probably not the correct way forward. Kapton is a versatile polymer though it may degrade at higher temperatures and humidity for a sufficiently long duration of time. Teflon is a suitable alternate, though it's bonding strength with metals is questionable. Performing further experiments will make known it's properties.

On Joining Methods Coming to the joining techniques, in this work, we explored adhesives for the joints between metals and polymers and also metals and metals. Laser bonding technique for joining metals and polymers was only partially explored in this study due to a lack of time and funds. But it will be very interesting to see how Copper and Kapton surface can be fused to form a strong bond. This requires finding suitable surface cleaning measures and careful mechanical alignment of tapes during the joining process. It is likely

to be a precarious affair. But once achieved, the benefits may be phenomenal. Results can be used in other parts of engineering as well.

6.2.2   On Adhesive Dispenser

In the current state of the manufacturing setup, we observe the occasional deviation of the tape from its intended position. This will, in turn, damage the contact between the tip of the mixer tube and top surface of the tape. Misalignments such as these could prove costly if not rectified in an industrial scenario. Besides, the use of more precise syringe pumps to accurately dispense milliliter volume of adhesive will help achieve finer control over bond width.

Due to the difference in viscosity between the epoxy resin and hardener, the mixing nozzle experiences unequal mixing. Lower viscosity fluid will dominate the y-section length and it becomes difficult to achieve the volumetric mixing ration recommended by the manufacturer. This problem requires more mathematical calculations as to the correct dispensing speeds and other control mechanisms.

6.2.3   On Surface Coatings

The current manufacturing system doesn't involve any kind of surface coatings. As mentioned at the beginning of this thesis, heat exchangers perform in a corrosive environment. In addition, there may internal salt deposition on the metallic surface due to industrial cold water. The use of metals directly in such an environment leads to fouling. Though the polymer sections of the heat exchanger reduce the amount of fouling this may not be sufficient in

the long run. We have worked with Energy Transport Research Lab at UIUC for developing coatings to protect the exposed metallic surface. Future work should involve embedding these coatings on the metallic surface either before or after the rolling of HX tubes.

6.2.4   On HX Testing

We used an existing wind tunnel to mimic the actual industrial situation to test heat transfer performance. There may be better ways to do this, such as building a custom inhouse setup with all the necessary instrumentation.

REFERENCES

[1] B. Incorporated, "Waste heat recovery: Technology and opportunities in u.s. industry," https://www1.eere.energy.gov/manufacturing/intensiveprocesses/pdfs/waste_heat_recovery.pdf, accessed: 2019-11-29.

[2] A. Thekdi and S. U. Nimbalkar, "Industrial waste heat recovery - potential applications, available technologies and crosscutting r&d opportunities," 2015.

[3] M. M. Awad, "Fouling of heat transfer surfaces," in *Heat Transfer*, A. Belmiloudi, Ed. Rijeka: IntechOpen, 2011, ch. 20. [Online]. Available: https://doi.org/10.5772/13696

[4] A. R. J. Hussain, A. A. Alahyari, S. A. Eastman, C. Thibaud-Erkey, S. Johnston, and M. J. Sobkowicz, "Review of polymers for heat exchanger applications: Factors concerning thermal conductivity," *Applied Thermal Engineering*, vol. 113, no. C, pp. 1118–1127, 2017.

[5] Nurazreena, L. B. Hussain, H. Ismail, and M. Mariatti, "Metal filled high density polyethylene composites electrical and tensile properties," *Journal of Thermoplastic Composite Materials*, vol. 19, no. 4, pp. 413–425, 2006. [Online]. Available: https://doi.org/10.1177/0892705706062197

[6] C. Aymonier, D. Bortzmeyer, R. Thomann, and R. Mlhaupt, "Poly(methyl methacrylate)/palladium nanocomposites: synthesis and characterization of the morphological, thermomechanical, and thermal properties," *Chemistry of Materials*, vol. 15, no. 25, pp. 4874–4878, 2003. [Online]. Available: https://doi.org/10.1021/cm031049h

[7] A. Roy, T. L. Bougher, R. Geng, Y. Ke, J. Locklin, and B. A. Cola, "Thermal conductance of poly(3-methylthiophene) brushes," *ACS Applied Materials & Interfaces*, vol. 8, no. 38, pp. 25 578–25 585, 2016, pMID: 27579585. [Online]. Available: https://doi.org/10.1021/acsami.6b04429

[8] X. Wang, V. Ho, R. A. Segalman, and D. G. Cahill, "Thermal conductivity of high-modulus polymer fibers," *Macromolecules*, vol. 46, no. 12, pp. 4937–4943, 2013. [Online]. Available: https://doi.org/10.1021/ma400612y

[9] C. L. Choy, Y. W. Wong, G. W. Yang, and T. Kanamoto, "Elastic modulus and thermal conductivity of ultradrawn polyethylene," *Journal of Polymer Science Part B: Polymer Physics*, vol. 37, no. 23, pp. 3359–3367, 1999.

[10] I. H. Tavman, "Thermal and mechanical properties of aluminum powder-filled high-density polyethylene composites," *Journal of Applied Polymer Science*, vol. 62, no. 12, pp. 2161–2167, 1996.

[11] M. C. Rajagopal, H. C. Chang, T. Man, G. Kuntumalla, Y. Meng, S. Sundar, H. Zhao, S. Salapaka, C. Shao, P. Ferreira, N. Miljkovic, and S. Sinha, "Materials-to-device design of hybrid metal-polymer heat exchanger tubes for low temperature waste heat recovery," *International Journal of Heat and Mass Transfer*, vol. 143, p. 118497, 2019. [Online]. Available: http://www.sciencedirect.com/science/article/pii/S0017931019325748

[12] G. Kuntumalla, Y. Meng, M. Rajagopal, R. Toro, H. Zhao, H. C. Chang, S. Sundar, S. Salapaka, N. Miljkovic, C. Shao, P. Ferreira, and S. Sinha, "Joining Techniques for Novel Metal Polymer Hybrid Heat Exchangers," vol. Volume 2B: Advanced Manufacturing, 11 2019, v02BT02A018. [Online]. Available: https://doi.org/10.1115/IMECE2019-10621

[13] B. Escaig, "Binding metals to polymers. A short review of basic physical mechanisms," *Journal de Physique IV Colloque*, vol. 03, no. C7, pp. C7–753–C7–761, 1993. [Online]. Available: https://hal.archives-ouvertes.fr/jpa-00251739

[14] K. Martinsen, S. Hu, and B. Carlson, "Joining of dissimilar materials," *CIRP Annals*, vol. 64, no. 2, pp. 679–699, 2015. [Online]. Available: https://app.dimensions.ai/details/publication/pub.1025349354andhttps://ntnuopen.ntnu.no/ntnu-xmlui/bitstream/11250/2450489/1/CIRP%2b1404_revised%2b2.pdf

[15] Y. Meng, D. Peng, Q. Nazir, G. Kuntumalla, M. C. Rajagopal, H. C. Chang, H. Zhao, S. Sundar, P. M. Ferreira, S. Sinha, N. Miljkovic, S. M. Salapaka, and C. Shao, "Ultrasonic Welding of Soft Polymer and Metal: A Preliminary Study," vol. Volume 2: Processes; Materials, 06 2019. [Online]. Available: https://doi.org/10.1115/MSEC2019-2938

[16] S. Fafenrot, N. Grimmelsmann, M. Wortmann, and A. Ehrmann, "Three-dimensional (3d) printing of polymer-metal hybrid materials by fused deposition modeling," *Materials*, vol. 10, no. 10, 2017. [Online]. Available: https://www.mdpi.com/1996-1944/10/10/1199

[17] N. R. Moody, E. D. Reedy, E. Corona, D. P. Adams, R. W. Friddle, M. S. Kennedy, M. J. Cordill, and D. F. Bahr, "Deformation and delamination in polymer metal thin film structures," https://www.osti.gov/servlets/purl/1140786, accessed: 2019-11-29.

[18] A. Al-Okaily, "Laser-driven micro-transfer printing for mems/nems integration," http://hdl.handle.net/2142/72946, accessed: 2019-11-29.

APPENDIX A - SOP FOR R2R MACHINE

Standard Operating Procedure

Roll-to-Roll (R2R) Manufacturing of Thin Film Hybrid Heat Exchangers

Procedure:

Initiation steps and wrap up steps are given separately for mechanical and electrical systems.

Mechanical:

1. Assemble the core of the circular mandrel by combining the four quarter cylinders together

2. Use the metal quadrants to cover the cylindrical structure assembled in step (1)

3. Use 2 hose clamps (one at each end) to hold the entire structure together. This is the final mandrel

4. Put the mandrel inside the 2 chucks of the rolling setup & clamp it at the ends

5. Load the copper and kapton tapes onto the tape holder (in the housing assembly)

6. Follow steps for case (i) or (ii) rolling (refer to DOE box folder for complete instructions with graphics). Starting points of tapes are different in these two cases

7. After rolling is complete, cut the overhanging tapes

8. Let the adhesive dry for 24 hours in case of epoxies and 5 minutes in case of silicone of acrylic

9. Collapse the mandrel by use of SS rod by tapping the inner quarter cylinders

10. Gently separate the Heat Exchanger from inner aluminum metal quadrants for further processing

11. **(wrap up)** Re-assemble metal quadrants and quarter cylinder rods to form the collapsible mandrel

Electronics:

1. Ensure that connections are intact and there are no loose contacts (by visual inspection)

2. Connect USB of the micro-controller to the R2R Laptop

3. (optional) Reset the positions of the linear actuators to zero. This step becomes necessary if some error occurs during standard operations

4. Connect the power supply to the main power source. Notice that the stepper motors start running and feel warm

5. Open the rolling machine software on the desktop (available in the Sinha Lab at UIUC) and verify if the terminal display shows ... interpreter enabled .. If yes, proceed to give commands

6. Typical commands look like

$$\$G01 \; X190 \; Y-128 \; Z190 \; F350 \qquad\qquad (A.1)$$

Where X, Y, Z correspond to positions and F is the feed rate and G01 is the default linear motion command in line with CNC standards

7. **(wrap up)** Zero the positions to home coordinates. default (x,y,z) = (0,0,0). Otherwise as determined by experimenters

8. **(wrap up)** Unplug USB and power connections

Safety:

1. Do not stop the linear actuators manually

2. If any issue occurs, unplug the **power supply** and **troubleshoot**

3. Do not use a feed rate more than F = 500

4. Precaution must be taken with respect to adhesives

   (a) Dont touch materials with bare hands. Use Nitrile gloves for protection

   (b) Dont let it drip on the floor. If it does, clean it with a wet tissue

   (c) In case of inhalation or ingestion, refer to the Material Safety Data Sheet (MSDS) available in the Sinha Lab. It is also available online

APPENDIX B - RAW PROGRAMS

The following Python codes were used for producing plots in the ASME IMECE 2019 conference paper titled "Joining techniques for novel metal polymer hybrid heat exchangers" and this thesis. Data files necessary to run the code are available at request with Prof. Sanjiv Sinha's laboratory at UIUC.

```python
#!/usr/bin/env python
# coding: utf-8


# In[1]:



#!/usr/bin/env python3
import numpy as np
import matplotlib.pyplot as plt
import pandas as pd
import math
import statistics as stats
import os
from scipy.interpolate import make_interp_spline, BSpline
import scipy.signal as sci_sg
def list_files(dir):
```

```python
17    r = []

18    direc = []

19    for root, dirs, files in os.walk(dir):

20        for name in files:

21            r.append(os.path.join(root, name))

22            if 'd1' in name:

23                direc.append(name)

24    return r, direc

25

26

27 # In[2]:

28

29

30 #Import data

31 root_dirc = r'C:\Users\gowtham4\Box\DOE_Research\Thermomechanical Testing\
     TM_test_data_April_4-16_2019\Adhesive_Apr_9'

32 r, direc = list_files(root_dirc)

33 data = []

34 calib_data = [ ]

35 titles= []

36 n = 0;

37 i=0

38 for i in range(0,np.size(r)):

39    if 'd1' in r[i]:

40        dataf = pd.read_csv(r[i],delimiter='\t', header = 0, index_col =
     None)

41        data.append(np.asarray(dataf.reset_index().values)[1:])
```

```python
42          titles.append(r[i])

43          n+=1

44          #print(r[i])




47  # In[3]:




50  # Rearranging test data

51  data_ar =[]

52  for xi in data:

53      data_ar.append(np.vstack(np.array(xi)).astype(np.float))

54  data_ar = np.array(data_ar)




57  # In[33]:




60  # Plotting Peel and Shear Tests

61  Peel_str = [] # nested list [ P test, T, avg value in N/cm, max, min]

62  Shear_str = [] # nested list [ S test, T, avg value in MPa, max, min]


64  TM_peel = ["AP","EP","SP"] # Thermomechanical test type

65  TM_shear = [ "AS","ES","SS"]

66  Temps = ['T1','T2','T3','T4'] # Temperatures = 22C, 100C, 150C, 200C

67  cvtT = {'T1':22,'T2':100, 'T3':150, 'T4':200}

68  clrs = ['b','r','g']
```

```python
69
70 for T in Temps:
71     for p_test in TM_peel:
72         expt_vals = []
73         test = str(p_test+'_'+T)
74         inds = [i for i in range(n) if test in titles[i]] # data indices
    for this test
75         if "AP_T1" in test:
76             inds.pop(0) #skip data point dure to error
77             inds.pop(0)
78
79         if "EP_T4" in test:
80             inds.pop(4) #skip data point dure to error
81
82         for j in inds:
83             X = data_ar[j][100:,0]-min(data_ar[j][:,0]) # zero the
    displacement
84             Y = 1000*(data_ar[j][100:,1]-min(data_ar[j][:,1]))  #Newtons
85             Y_fit = sci_sg.savgol_filter( Y, 49, 5 )   # Savitzky Golay
    filter for improving SNR
86             expt_vals.append(round(max(Y_fit)/2.54,2))  #N/cm
87         Peel_str.append([test,cvtT[T],round(sum(expt_vals)/len(expt_vals)
    ,2), max(expt_vals),min(expt_vals),stats.stdev(expt_vals)])
88
89     for s_test in TM_shear:
90         expt_vals = []
91         test = str(s_test+'_'+T)
```

```
92          inds = [i for i in range(n) if test in titles[i]] # data indices
   for this test
93          for j in inds:
94              X = data_ar[j][:,0]-min(data_ar[j][:,0]) # zero the
   displacement
95              Y = 1000*(data_ar[j][:,1]-min(data_ar[j][:,1]))  #Newtons
96              Y_fit = sci_sg.savgol_filter( Y, 25, 5 )   # Savitzky Golay
   filter for improving SNR
97              if "ES" not in test: # different sample sizes
98                  expt_vals.append(round(max(Y_fit)/(2.54*5*100),2))  #MPa
99              else:
100                 expt_vals.append(round(max(Y_fit)/(2.54*3*100),2))
101         Shear_str.append([test,cvtT[T],round(sum(expt_vals)/len(expt_vals)
   ,2), max(expt_vals),min(expt_vals),stats.stdev(expt_vals)])
102
103
104 # In[34]:
105
106
107 clors = ['k', 'g', 'b', 'c']
108 linsty = ['--o', '-.o', ':o', '-o']
109 cvtAdh = {"AP":"Acrylic","AS":"Acrylic","EP":"Epoxy","ES":"Epoxy","SP":"
   Silicone","SS":"Silicone"}
110 Temps = [22,100,150,200] # Temperatures
111
112 j= 0
113 plt.figure()
```

```python
114  for test in TM_peel:
115      inds = [i for i in range(len(Peel_str)) if test in Peel_str[i][0]]
116      X = [Peel_str[i][1] for i in inds]
117      Y = [Peel_str[i][2] for i in inds]
118      c = [round((Peel_str[i][2] - Peel_str[i][3]),2) for i in inds]
119  #     c = [Peel_str[i][4]for i in inds] # std
120      plt.errorbar(X,Y, yerr = c, linestyle = linsty[j][:-1], fmt ='-o'+
         clors[j],ecolor= clors[j],
121          mfc = clors[j],capsize= 5, label = (cvtAdh[test]))
122      j = j+1
123      print()
124  plt.xlabel("Temperature "+ '($^\circ C$)')
125  plt.ylabel("Peel (Tensile) Strength (N/cm)" )
126  plt.legend(fontsize = 10, loc = 1)
127
128
129  fname = root_dirc +"\\Peel_str_april16"+ ".jpg"
130  plt.savefig(fname, format = 'jpg', dpi = 500 )
131  plt.show()
132
133
134
135  plt.figure()
136  j = 0
137  for test in TM_shear:
138      inds = [i for i in range(len(Shear_str)) if test in Shear_str[i][0]]
139      X = [Shear_str[i][1] for i in inds]
```

```python
140     Y = [Shear_str[i][2] for i in inds]

141     c = [round((Shear_str[i][3] - Shear_str[i][4])/2,2) for i in inds]

142 #      c = [Shear_str[i][4]for i in inds] # std

143     plt.errorbar(X,Y, yerr = c, linestyle = linsty[j][:-1], fmt ='-o'+
    clors[j],ecolor= clors[j],

144         mfc = clors[j],capsize= 5, label = (cvtAdh[test]))

145     j = j+1

146     print()

147 plt.xlabel("Temperature "+ '($^\circ C$)')

148 plt.ylabel("Shear Strength (MPa)" )

149 plt.legend(fontsize = 10, loc = 1)

150

151

152 fname = root_dirc +"\\Shear_str_april16"+ ".jpg"

153 plt.savefig(fname, format = 'jpg', dpi = 500 )

154 plt.show()

155

156

157

158 ###################################

159

160 # plt.axhline(y = 3.9, color='r', linestyle='-',label = 'Proposal')

161 # plt.axhline(y = y_calib/1.5, color='y', linestyle='--',label = '
    calibration er')

162 # plt.xticks(fontsize = 15)

163 # plt.yticks(fontsize = 15)

164
```

```python
165

166  # In[26]:

167

168

169  ar=0

170  while ar<len(data_ar):

171      plt.figure()

172      plt.xlabel("Displacement(mm)")

173      plt.ylabel("Load (N)")

174      X = data_ar[ar][100:,0]-min(data_ar[ar][100:,0])

175      Y_a = 1000*(data_ar[ar][100:,1] - min(data_ar[ar][100:,1]))

176      Y = sci_sg.savgol_filter( Y_a, 49, 5 )

177      plt.plot(X,Y,label = cvtT [T],color  ='r')

178      if "AP_T4_2d1" in titles[ar]:

179          fname = root_dirc +"\\adhAc_peel_load_curve"+ ".jpg"

180          plt.savefig(fname, format = 'jpg', dpi = 500 )

181      if "ES_T3_2d1" in titles[ar]:

182          fname = root_dirc +"\\adhEp_shear_load_curve"+ ".jpg"

183          plt.savefig(fname, format = 'jpg', dpi = 500 )

184      plt.title(titles[ar][-15:])

185      ar+=1

186

187

188  # In[21]:

189

190

191  for i in range(len(Peel_str)):
```

```
192     print (Peel_str[i],'\n')

193 for i in range(len(Peel_str)):

194     print (Shear_str[i],'\n')

195

196

197 # # Code ends here
```

The following Python code was used for producing Shear strength plots for Epoxy adhesives. Data files necessary to run the code are available at request with Prof. Sanjiv Sinha's laboratory at UIUC.

```
1 #!/usr/bin/env python

2 # coding: utf-8

3

4 # In[1]:

5

6

7 import numpy as np

8 import matplotlib.pyplot as plt

9 import csv

10 import math

11 import os

12 import xlrd # for excel sheets

13

14

15 # In[2]:

16

17
```

```python
18 def list_files(dir):

19     r = []

20     direc = []

21     for root, dirs, files in os.walk(dir):

22         for name in files:

23             r.append(os.path.join(root, name))

24             if 'Results' in name:

25                 direc.append(name)

26     return r, direc

27

28

29 # In[3]:

30

31

32 def get_str (file):

33     strength = 0

34     with open(file) as csv_file:

35         csv_reader = csv.reader(csv_file, delimiter=',')

36         line_count = 0

37         for row in csv_reader:

38             line_count+=1

39             if line_count == 8:

40                 strength = row[5]

41     return strength

42

43

44 # In[4]:
```

```
45

46

47  #Import max shear strength data

48  root_dirc = r'C:\Users\gowtham4\Box\DOE_HX\Data_experiments\
        Thermomechanical Testing\Epoxy_Sep20_to_Oct4_2019\
        Sinhalab_Epoxy_Shear_Tests'

49  r, direc = list_files(root_dirc)

50  types = ['CuK','CuCu'] # K is Kapton

51  adh_list = ['KW','CW','PB','CO']

52  temps = ['T1','T2','T3']

53  reps =['_1','_2','_3','_4','_5'] # repetitions

54

55  CuK_shear_str = np.zeros((len(adh_list),len(temps),len(reps))) # 4 adh x
        (3 temps x 5 reps)

56  CuCu_shear_str = np.zeros((len(adh_list),len(temps),len(reps))) # 4 adh x
        (3 temps x 5 reps)

57

58  for i in range(np.size(r)):

59      if 'Results' in r[i]:

60          shear_str = get_str(r[i])

61

62          for sample in types:

63              if sample in r[i]:

64                  a = types.index(sample)

65                  for adh in adh_list:

66                      if adh in r[i]:

67                          b = adh_list.index(adh)
```

74

```python
                        for T in temps:
                            if T in r[i]:
                                c = temps.index(T)
                                for rep in reps:
                                    if T+rep in r[i]:
                                        d = reps.index(rep)
                                        break
                                break
                            break
                    break

        # assign value in array


        if a == 0:
            CuK_shear_str[b][c][d] = round(float(shear_str),2)
        if a == 1:
            CuCu_shear_str[b][c][d] = round(float(shear_str),2)
    else:
        continue


# print(CuK_shear_str)
# print(CuCu_shear_str)



# In[5]:


```

```python
95  # temps
96  temps_file = r'C:\Users\gowtham4\Box\DOE_HX\Data_experiments\
        Thermomechanical Testing\Epoxy_Sep20_to_Oct4_2019\real_temperature.xlsx
        '
97
98  typess = ['Cu_K','Cu_Cu'] # K is Kapton
99
100 wb = xlrd.open_workbook(temps_file)
101
102 T2_temps = np.zeros((2, len(adh_list), 2, len(reps))) # CuK,CuCu x (4 adh
        x (Front,Back x 5 reps))
103 T3_temps = np.zeros((2, len(adh_list), 2, len(reps)))
104
105 sheet_lst = wb.sheet_names()
106
107 for sht in sheet_lst:
108     sheet = wb.sheet_by_name(sht)
109     for t in typess:
110         if t in sht:
111             a = typess.index(t)
112             for adh in adh_list:
113                 if adh in sht:
114                     b = adh_list.index(adh)
115                     for m in range(2):
116                         for n in range(len(reps)):
117                             T2_temps[a,b,m,n] = sheet.cell_value(1+n,2+m)
        # look at the real_temperature excel
```

```
118                                    T3_temps[a,b,m,n] = sheet.cell_value(7+n,2+m)

119                        break

120             break

121

122 #print (T2_temps,'\n\n', T3_temps)

123

124 #print(sheet_lst)

125

126

127 # In[10]:

128

129

130 ## Plotting Results

131

132 clrs = ['r','b','g','y']

133 linsty = ['--', '-.', ':', '-']

134 adh_names = ["JB Kwik Weld","JB Cold Weld", "JB Plastic Bonder", "
        Cotronics 4538"]

135

136 ### Copper/ Kapton Joints ###

137

138 for i in range(4):

139     # plt.plot(range(3),np.mean(CuK_shear_str[i][:][:],axis = 1), clrs[i],
          marker ='o',label = adh_list[i], linestyle = linsty[i])

140     x_means = np.array([25,np.mean(T2_temps[0][i][:][:],axis = 1)[0],np.
        mean(T3_temps[0][i][:][:],axis = 1)[0]])

141     x_errs = np.array([2,0.5*(np.max(T2_temps[0][i][:][:],axis = 1)[0]-np.
```

```python
      min(T2_temps[0][i][:][:],axis = 1)[0]),0.5*(np.max(T3_temps[0][i
      ][:][:],axis = 1)[0]-np.min(T3_temps[0][i][:][:],axis = 1)[0])])
142    y_means = np.mean(CuK_shear_str[i][:][:],axis = 1)

143

144    # range based error bar
145    y_errs = np.array([0.5*(np.max(CuK_shear_str[i][j][:])- np.min(
      CuK_shear_str[i][j][:])) for j in range(len(temps))])

146

147    # minmax based error bar
148 #     y_errs = np.asarray([np.min(CuK_shear_str[i][j][:]) for j in range(
      len(temps))])
149 #     y_errs = np.append(y_errs,np.asarray([np.max(CuK_shear_str[i][j][:])
       for j in range(len(temps))]),axis =0)
150 #     y_errs = np.array(y_errs).reshape(2,len(temps))
151    plt.errorbar(x_means,y_means,yerr = y_errs, xerr = x_errs,linestyle =
      linsty[i], fmt ='-o'+clrs[i],ecolor= clrs[i],
152              mfc = clrs[i], capsize= 5, label = adh_names[i])

153

154 plt.axhline(y=0.74, color='c', linestyle='--', label = '5 mil Kapton
      Tensile')
155 plt.axhline(y=0.1, color='k', linestyle='--', label = '0.1 MPa limit')
156 plt.title("Shear Strength vs. Temperature in Copper/Kapton Joints")
157 plt.xlabel("Temperature ( C )")
158 plt.ylabel("Strength (MPa)")
159 plt.legend()
160 fname = r'C:\Users\gowtham4\Box\DOE_HX\Data_experiments\Thermomechanical
      Testing\Epoxy_Sep20_to_Oct4_2019\\'+ 'CuK_Shear_Results'+'.jpg'
```

```python
161 plt.savefig(fname, format = 'jpg', dpi = 600 )

162 plt.show()

163

164

165 ### Copper/ Copper Joints ###

166

167

168 for i in range(4):

169     #plt.plot(range(3),np.mean(CuCu_shear_str[i][:][:],axis = 1), clrs[i],
             marker ='o', label = adh_list[i], linestyle = linsty[i])

170     x_means = np.array([25,np.mean(T2_temps[1][i][:][:],axis = 1)[0],np.
        mean(T3_temps[1][i][:][:],axis = 1)[0]])

171     x_errs = np.array([2,0.5*(np.max(T2_temps[1][i][:][:],axis = 1)[0]-np.
        min(T2_temps[1][i][:][:],axis = 1)[0]),0.5*(np.max(T3_temps[1][i
        ][:][:],axis = 1)[0]-np.min(T3_temps[1][i][:][:],axis = 1)[0])])

172     y_means = np.mean(CuCu_shear_str[i][:][:],axis = 1)

173

174     # range based error bar

175     y_errs = np.array([0.5*(np.max(CuCu_shear_str[i][j][:])- np.min(
        CuCu_shear_str[i][j][:])) for j in range(len(temps))])

176

177     # minmax based error bar

178 #     y_errs = np.asarray([np.min(CuCu_shear_str[i][j][:]) for j in range(
        len(temps))])

179 #     y_errs = np.append(y_errs,np.asarray([np.max(CuCu_shear_str[i][j
        ][:]) for j in range(len(temps))]),axis =0)

180 #     y_errs = np.array(y_errs).reshape(2,len(temps))
```

```python
181    plt.errorbar(x_means,y_means,yerr = y_errs, xerr = x_errs,linestyle =
        linsty[i], fmt ='-o'+clrs[i],ecolor= clrs[i],
182                 mfc = clrs[i], capsize= 5, label = adh_names[i])
183 plt.axhline(y=0.1, color='k', linestyle='--', label = '0.1 MPa limit')
184 plt.title("Shear Strength vs. Temperature in Copper/Copper Joints")
185 plt.xlabel("Temperature ( C )")
186 plt.ylabel("Strength (MPa)")
187 plt.legend()
188 fname = r'C:\Users\gowtham4\Box\DOE_HX\Data_experiments\Thermomechanical
        Testing\Epoxy_Sep20_to_Oct4_2019\\'+ 'CuCu_Shear_Results'+'.jpg'
189 plt.savefig(fname, format = 'jpg', dpi = 600 )
190 plt.show()
```